# The microalga Volvox carteri as a cell supportive building block for tissue engineering

**Mathilde STRICHER**
UTC: Universite de Technologie de Compiegne
**Pascale Vigneron**
UTC: Universite de Technologie de Compiegne
**Frédéric Delbecq**
ESCOM: Ecole superieure de chimie organique et minerale
**Claude-Olivier Sarde**
UTC: Universite de Technologie de Compiegne
**Christophe Egles**
christophe.egles@univ-rouen.fr

Université de Rouen: Universite de Rouen Normandie https://orcid.org/0000-0003-0982-7752

**Research Article**

**Keywords:** Algal extracellular matrix, Vegetal alternative, Modular self-assembly tissue engineering, Soft tissue augmentation, Adipogenesis

**Posted Date:** November 14th, 2023

**DOI:** https://doi.org/10.21203/rs.3.rs-3484389/v1



**Version of Record:** A version of this preprint was published at Materials Today Bio on April 1st, 2024. See the published version at https://doi.org/10.1016/j.mtbio.2024.101013.

# Abstract

### Background

*V. carteri f. nagariensis* constitutes, in its most simplified form, a cellularized spheroid built around and stabilised by a form of primitive extracellular matrix (ECM).

### Methods

Based on its structure and its ability to support surface cell adhesion most likely induced by the composition of its algal ECM, we have developed a modular approach to soft tissue engineering by compact-stacking of *V. carteri*–based living building blocks.

### Results

A primary biocompatibility assessment demonstrated the algal suspension cytocompatibility, its histogenesis promoting properties, and that it did not induce an inflammatory response *in vitro*. These results allowed us to consider the use of such algal suspension for soft tissue augmentation and to initiate the study of its *in vivo* biocompatibility. *V. carteri* exhibited cellular fate-directing properties, causing fibroblasts to take on an alkaline phosphatase$^{+}$ stem-cell-like phenotype and both human adipose-derived stem cells and mouse embryonic stem cells to differentiate into preadipocytes to adipocytes. The ability of *V. carteri* to support histogenesis and adipogenesis was also observed *in vivo* by subcutaneous tissue augmentation of athymic mice, highlighting the potential of *V. carteri* to support or influence tissue regeneration.

### Conclusions

Our conclusion present for the first time *V. carteri* as an innovative and inspiring biomaterial for tissue engineering and soft tissue regeneration. Its strategies in terms of shape, structure and composition can be central in the design of a new generation of bio-inspired heterogeneous biomaterials recapitulating more appropriately the complexity of the body tissues when guiding their regeneration.

# 1. Background

Over the past years, tissue engineering strategies have gradually shifted away from the conventional top-down approach of scaffold cellularization to a more malleable modular design based on coupled individual living building blocks (LBB). In this approach, LBB of varying complexity are combined via self, directed, or remote assembly principles in various dimensions and geometries (e.g., cell fibers, cell sheets, and spheroids), optionally including biomaterials and biomolecules (1). This design allows for a more facilitated and controlled introduction of progressive heterogeneity (e.g., zonal or gradient seedings and substrate transitions) and structural complexity (e.g., vascular or neuronal networks and specific microstructures) that more accurately mimics true *in vivo* tissue environments.

The modular approach is thus founded on the notion that progressive multicellularity promotes efficiently the emergence of a complex organization. This concept is widely shared in the evolutionary community as the acquisition of multicellularity constitutes one of the major transitions towards complexity in evolution (2). Although transitions from single-celled organisms to multicellular ones have occurred multiple times independently throughout evolution, that carried out by the green algae volvocine has been one of the most studied and is considered a remarkable model to decipher the genetic bases of multicellularity and cell differentiation (3).

Indeed, volvocine algae represent a unique evolutionary continuum in the acquisition of multicellularity, which extends from the unicellular organism *Chlamydomonas reinhardtii* to the multicellular alga *Volvox carteri* which represents its most advanced manifestation. Their phylogenomic analysis, initiated by Kirk (4), defines a progressive acquisition of fundamental processes (e.g., cell-cell adhesion, organism polarity, extracellular matrix (ECM) expansion, and cell differentiation mechanisms) that have been widely agreed upon and continuously refined ever since (5, 6).

*V. carteri*, like other green algae, can be found worldwide, particularly in low-turbulent, low-turbidity, high-alkalinity, and nutrient-rich freshwater ecosystems (7, 8). An adult spheroid represents a 100 to 500 µm algal ECM-based sphere comprising an outer sheet, consisting of a monolayer of ∼2000–4000 equidistant biflagellate somatic cells whose general appearance is reminiscent of their distant ancestor *Chlamydomonas*, and enclosing ∼16 much larger reproductive aflagellated gonidia cells.

During its growth, each alga produces a considerable amount of ECM, accounting for up to 99% of its total volume and forming a continuum of zones that seem defined by specific molecular compositions. (9). The algal ECM is however primarily composed of negatively charged fibrous hydroxyproline-rich glycoproteins (HRGP), mainly Volvocale-specific glycoproteins termed “pherophorins” (10). On account of their hydroxyproline-rich composition, fibrillar structure, and function as crosslinking and scaffolding proteins, pherophorins are considered analogous to animal collagen in the building of ECM architectures (13).

In a primary biomimicry and bioinspiration initiative driven by the necessity to develop plant alternatives to animal-derived products for tissue engineering, we have studied the potential of *V. carteri* to respond to this challenge. After ascertaining its overall biocompatibility, we developed a modular approach to soft tissue engineering of compact stacking using animal cell-seeded *V. carteri f. nagariensis* spheroids as living building blocks. We demonstrated that this microalga displays a cell adhesive glycoprotein-based scaffold which supports histogenesis, and is able to direct adipogenesis both *in vitro* and *in vivo*.

# 2. Methods

Unless otherwise stated, culture reagents were purchased from GibcoTM (ThermoFisher Scientific, Waltham, MA, USA),l primary cells and lineages were provided by ATCC (Manassas, VA, USA) and cultured in 4.5 g/L glucose Dulbecco’s modified eagle’s medium (DMEM), supplemented with 10% V/V decomplemented Fetal Bovine Serum (FBS), 100 U/mL penicillin, 100 µg/mL streptomycin, and 2 mM of

L-Glu. Characterized FBS (HyClone, Logan, UT, USA) was used for primary neonatal Human Dermal Fibroblasts (HDFn) culture. Human Umbilical Vein Endothelial Cells (HUVEC) were cultured in M199 medium, 10%V/V FBS, 50 µg/mL of heparin B, 2 mM of L-Glu, 100 units/ml of penicillin, and 100 µg/ml of streptomycin. Human adipose-derived mesenchymal stem cells (hASC) were maintained in Mesenchymal Stem Cell (MSC) basal medium enriched with MSC supplement (ATCC, Manassas, VA, USA), 100 units/mL of penicillin and 100 µg/mL of streptomycin.

## 2.1. *V. carteri* culture and processing

*V. carteri f. nagariensis* (NIES397) was provided by NIES based in Tsukuba, Japan. This algal strain was grown continuously in 300 mL batch culture under sterile conditions in VT medium pH 7.5 at 25°C under an alternating 14:10 hrs day-night cycle in a growth chamber fitted with a 15000-lux light system (POL-EKO-APARATURA, Wodzisaw Sski, Poland) (14). On the 19th day of culture, spheroids were harvested by filtration using a 100 µm porosity sieve (Haver & Boecker oHG, Oelde, Germany). The algal suspension was either freshly used or preserved with 70% ethanol or 4% paraformaldehyde (PFA). The algal culture was regularly observed and enumerated, whether fresh, preserved, or immobilized in a 200 mM acid acetic solution in a Sedgewick Rafter S52 counting cell (Graticules Optics Ltd., UK). *V. carteri* extracts were produced by crushing 15 000 spheroids/mL of PBS suspension with a UP400S ultrasonic device (Hielscher Ultrasonics, Teltow, Germany) using 0.5 second cycles at 400 W and 24 kHz for 1 min. After 1 min of 3500 Relative Centrifugal Force (RCF) centrifugation, the soluble fraction was collected and filtered at 0.8 µm.

## 2.2. Investigation of *V. carteri* adequacy as a substrate for *in vitro* cell culture

*Cytotoxicity investigation* was adapted from the ISO 10993-5 standards: A first testing extract was prepared by incubating rinsed, 70% ethanol-fixed spheroids for 24 hrs at 37°C with agitation in a 1:1 algal pellet:culture medium ratio. The second extract of fresh *V. carteri* spheroids pellet was produced in culture medium and ultrasonically crushed on ice as previously described. L929 mouse fibroblast (ATCC-CC1-1) monolayers pre-cultured in 96-well plates for 24 hrs at 37°C with 5% CO2 were treated for an additional 24 hrs with 100 µL of testing extract. L929 mitochondrial activity was quantified after a 2-hr incubation in 3-(4,5-dimethylthiazol-2-yl)-5-(3-carboxymethoxyphenyl)-2-(4-sulfophenyl)-2H-tetrazolium (MTS) solution (1:5; Promega, Madison, WI, USA). Cellular viability was determined as the 492 nm-absorbance ratio of the extract to the untreated control. The validity of the experiment was assessed using a latex containing material known to be cytotoxic. A material inducing more than 70% cellular viability was deemed non-toxic.

### In vitro inflammation analysis

The inflammatory pattern of the J774 murine macrophage lineage (ECACC-85011428) was determined after a 24-hr exposure to freshly harvested, 70% ethanol-fixed and rinsed raw *V. carteri* spheroids or to 0.8 µm-filtered *V. carteri* extracts. J744 macrophages were seeded at a density of 200 000 cells per well in a

12-well plate and incubated overnight. Macrophages were exposed at a density of 15,000 *V. carteri* spheroids/mL or equivalent. Negative and positive control conditions were generated through exposure to a culture medium alone or with a concentration of 20 µg/mL of lipopolysaccharide toxin (LPS). Supernatants were recovered the following day and stored at -20°C. The supernatants cytokines and chemokines concentrations (pg/mL) were quantified using the V-plex Proinflammatory Panel 1, Cytokine Panel 1, and Th17 Panel 1 kits from Meso Scale Diagnostics (MSD, MD, USA) according to the manufacturer's instructions. These values were replaced by the threshold values for concentrations below or above the detection limits. The concentrations were expressed as a log2-fold change from the untreated control. To identify the main axes of variance and different patterns within this multidimensional data set, the data was processed under principal component analysis following an autoscaling normalization using Metaboanalysis software.

*α-D-mannosyl and α-D-glucosyl-containing glycans and glycoproteins Concanavalin A (ConA) lectin staining*: 4% PFA-fixed *V. carteri* spheroids were prepared for staining by performing two 10-minute PBS washes, a 10-minute 5% V/V Triton X100 permeabilization, a 5-minute PBS wash, and a 15-minute 3% w/v Bovine Serum Albumin (BSA) non-specific site saturation. Concanavalin A Alexa Fluor™ 488 (ConA AF 488, Invitrogen™, Waltham, MA, USA) labeling was then pursued according to manufacturer's instructions and observed using confocal microscopy (Zeiss LSM 710, Zeiss, Jena, Germany).

### Estimation of the cell adhesive properties of V. carteri

non-adhesive 6-well plates (Evergreen Scientifics, Vernon, CA, USA) were precoated with 1 mL of *V. carteri* extract per well for 1 hr at 37°C. The cell suspensions of HDFn (C-004-5C) and HUVEC (CRL-1730TM) were then seeded at a density of 5 000 cells/cm2 on a non-adhesive or algal extract pre-coated surface. Cell confluency was evaluated at 24 and 48 hrs on contrast-phase light microscopic acquisitions using Image J and the PHANTAST plugin.

### Estimation of V. carteri spheroids' in vitro stability and deformability

500 µL of saturated algal suspension was placed in 12-well culture inserts (353181, Falcon™, Corning, NY, USA). The sample was maintained in the same condition as cellularized samples would be (i.e., 37°C, 5% $CO_2$ for 21 culture days with regular basal media changes). The deformability of the algae was monitored by phase-contrast microscopy imaging on days 2, 7, 14, and 21. The circularity of each colony was determined using Image J and calculated as follows

$$Circularity = 4\pi \times \frac{Area}{Perimeter^2}$$

1.1

A perfectly circular colony would have a circularity index of 1.

## 2.3. *V. carteri* predicted proteome human ECM sequence homology screening

Using *V. carteri*'s previously published EuKaryotic Orthologous Groups (KOG) annotation analysis and predicted proteome [23], BlastP sequence homology analyses were performed on a set of proteins annotated as extracellular against human extracellular matrix basic constituent sequences. Significant sequence homologies and identities were considered when $10^{-50} \leq$ E-value $< 10^{-02}$ and when E-value $< 10^{-50}$.

## 2.4. Macrotissue formation using the compact stacking of seeded *V. carteri*-based living building block

The seeded *V. carteri*-based LBB and subsequent microtissue formation process were standardized for the following cell types: L929, HDFn, HUVEC, C3H10 (ATCC-CCL-226), and ASC (ATCC SCRC-4000).

*Formation of seeded V. carteri-based living building blocks*: Ethanol 70%-preserved *V. carteri* suspension was twice washed in PBS, allowing spheroids to sediment at 4°C in between washes. The algae were then primed overnight (ON) with the culture medium associated with the cell to be seeded. *V. carteri*-based LBB were formed by homogenizing a cell suspension of 2 $10^6$ cells/mL with a saturated algae suspension at a volume of 1:1 ratio, incubating the mix for 45 min in a 15-mL tube and then for 4 hrs on a non-cell adhesive petri dish (Greiner Bio-One, Frickenhausen, Germany) or 6-well plate (Evergreen Scientifics, Vernon, CA, USA).

#### Self-assembly of seeded V. carteri-based living building blocks into macrotissue

The seeded *V. carteri*-based LBB suspension was transferred at 1 mL per 12-well culture insert in 3-µm porosity-culture inserts (353181, Falcon™, Corning, NY, USA). Except for the L929 lineage which required 0.4-µm porosity-culture inserts (353180, Falcon™, Corning, NY, USA). The construct was provided with 1 mL of culture medium in the basal compartment daily, changed for 2 days to remove the excess medium, and then every 2–3 days until 21 days of culture. The samples were either processed immediately or fixed with 4% PFA for 1 hr at 37°C, depending on the subsequent analysis performed.

## 2.5. Characterization of seeded *V. carteri*-based living building blocks and microtissue

#### Seeded V. carteri-based living building blocks (LBB) observation

The LBB were observed routinely directly on non-adhesive surface using contrast-phase microscopy. L929 seeded *V. carteri*-based LBB were additionally examined with an environmental scanning electron microscope upon brief rinsing and subsequent 3% glutaraldehyde in Rembaum buffer (pH 7.4) 1 hr fixation.

### Cellular activity monitoring

As previously described, HDFn-seeded *V. carteri*-based LBB were produced and cultured in 24-well culture inserts (3 µm porosity, 353104, Falcon™, Corning, NY, USA). At days 2, 7, 14, and 21, cellular proliferation was monitored by quantifying HDFn mitochondrial activity using MTS testing. The 492 nm absorbance of the MTS solution was therefore measured after a 2-hour incubation at 37°C, while inverted contrast-phase microscopy observations were carried out in parallel. Similarly, the alkaline activity of HDFn phosphatase was measured by contrast-phase microscopy after 1 hour of incubation in 1 mL of BCIP®/NBT Liquid Substrate System (Sigma-Aldrich, St. Louis, MO, USA) at 37°C in the dark.

*Histology*: Classical sample preparation, hematoxylin-eosin (HE), and optional safran (HES) staining procedures were applied. To better distinguish the contours of the algal spheroids in the formed macrotissue, *V. carteri* spheroids surface was coupled with rhodamine-NHS (Life Technologies, Carlsbad, CA, USA) according to the manufacturer's recommendations prior to cell seeding and 21-day culture. Rhodamine-coupled macrotissues were also processed for conventional HES staining. Human cells were counterstained with DAPI and observed via epifluorescence microscopy (Leica Microsystems, Wetzlar, Germany). Adipogenic differentiation was monitored on days 2, 7, 14, and 21 of culture on *V. carteri*-based LBB or macrotissues produced with either adipose-derived or C3H10 embryonic stem cells, staining eventual lipid droplets using Oil Red O. All solutions were deposited in the basal compartment to avoid dispersion of the sample. After 1 hour of 4% PFA fixation at 37°C, the sample was rinsed twice in osmotic water for 15 minutes before incubating ON at RT with 1 mL of 1.5 mg/mL Oil Red O working solution. The residual dye was rinsed out thoroughly. Following a 1-minute hematoxylin staining, the samples were counterstained for bright-field microscopy observation. For confocal microscopy observation, the samples were counterstained for 30 minutes in a 1 µg/mL DAPI solution at RT in the dark and washed in PBS for additional 15 minutes. The macrotissues were then prepared for Phalloidin-iFluor 488 ON staining (1:1000, Abcam, Cambridge, UK) and DAPI counterstaining by successive 10-minute 0.1% triton X100 permeabilization, 15-minute 3% BSA saturation, and 15-minute rinsing using osmotic water. The sample was isolated from the insert membrane and transferred to a standard microscope slide or an imaging chamber coverslip (Ibidi, Gräfelfing, Germany) for observation.

## 2.6. Implantation in a Model of Athymic Mice

All experiments were realized in compliance with European Directive 2010-EU63 and the ARRIVE guidelines. The study design, the sample size, the outcomes and the experimental procedures were approved by the "Comité Régional d'Ethique en Matière d'Expérimentation Animale de Picardie" (CREMEAP; C2EA-96). The chosen experimental animals were pathogen-free 5-week-old male athymic mice (Rj: NMRI-Foxn1 nu/nu, JANVIER LABS, Le Genest-Saint-Isle, France; 30 g). Animal were housed in polycarbonate cages in a temperature- and humidity-controlled room and had food and water ad libitum. Both 70% ethanol-preserved *V. carteri* saturated suspension and HDFn-seeded *V. carteri* LBB-based macrotissue samples were implanted subcutaneously on the backs of athymic mice. The animals were euthanized after one or two months, and their back skin was harvested, observed under a microscope,

and processed under classical histology procedures (Althisia, Troyes, France) for an anatomopathological read-out by a certified professional.

# 3. Results

## 3.1. Production of *V. carteri* microalgae material on a laboratory scale

*Volvox carteri* was grown axenically in a batch culture system that allowed for the production of 2.52 ± 0.61 million spheroids per liter of medium. This system provided a sufficient, continuous, and regular supply of fresh microalgae material, with maximum production in the growth chamber reaching 151 ± 36.6 million *V. carteri* spheroids per batch. The algal culture being unsynchronized in our culture conditions, the harvested suspension contained algal spheroids at every developmental stage (Fig. 1.A), ranging from juvenile spheroids sheltering unicellular gonidia to mature spheroids about to hatch and degenerate upon next generation release.

The incorporation of the *V. carteri* microalga into mammalian cell cultures with the aim of using it as cell support material required preserving their structure as much as possible by fixing, which implied stopping their proliferation, as well as cellular and metabolic activities as quickly as possible and thus limiting any stress response. 4% PFA preservation showed overall maintenance of the microalga's integrity, structure, and composition, but its use was ultimately limited to the algae structural study as cytotoxic releases were observed despite numerous successive washings (data not shown). Histochemical staining with concanavalin A (Fig. 1.B) demonstrated the omnipresence of α-D-mannose and α-D-glucose in glycans and glycoproteins present in cells, cytoplasmic membranes and extracellular material. It particularly highlighted the fundamental involvement of the ECM in the composition, formation and cohesion of the structure of algae. The 70% ethanol fixation appeared to partially deflagellate the outer somatic cells, to permeabilize the colony membrane, releasing small soluble compounds including chlorophyll pigments, and to preserve the overall algal geometry. As a less harmful and more easily eliminated solvent, capable of preserving the algal overall integrity and sterility for up to a year (data not shown), 70% ethanol preservation was thus preferred for the subsequent formation of *V. carteri* LBB-based macrotissue, whose process is described in Fig. 1.C.

The cellular reactivity to *V. carteri*'s introduction as a culture substrate was investigated by analyzing cellular activity and dynamics upon direct contact.

## 3.2. Evaluation of V. carteri in vitro biocompatibility: cytotoxicity and inflammation

The cytocompatibility of *V. carteri* primed and sonicated medium was determined using the ISO 109933-5 standard recommendations. L929 murine fibroblasts' cellular viability was determined following a 24-hour exposure (Fig. 2.A). For *V. carteri* primed medium (i.e., mimicking the contact with the surface of the

alga), a L929 viability of 99.8 ± 8.8% was obtained, while for the sonicated condition (i.e., simulating the full algal compound exposure, both external and internal), a L929 cell viability of 94.2 ± 9.3% was found. Thus, all *V. carteri* conditions demonstrated L929 viability above the 70% threshold. According to ISO 10993 criteria, the algal suspension and extract are considered non-cytotoxic.

The murine J774.2 macrophage cytokine secretome heatmap (Fig. 2.B) was generated after a 24-hour exposure to various *V. carteri* samples in comparison to untreated (CTRL-) and pro-inflammatory LPS-treated (CTRL+) controls to further assess its biocompatibility. This heatmap highlights an expected acute inflammation induced by 2 µg/mL LPS exposure through the significant secretion of numerous pro-inflammatory cytokines. This pro-inflammatory response was also evidenced via principal component analysis (PCA, Fig. 2.C), as the LPS-treated condition represents a cluster isolated from the untreated condition. *V. carteri* samples did not show pro-inflammatory cytokine and chemokine secretions to the extent induced by LPS, as shown by the heatmap profiles and the aggregation of the algal samples around the negative control on the PCA. Only freshly harvested, unfixed *V. carteri* spheroids induced moderate IL-6 and TNF-α secretions.

In the PCA provided as supplementary material (Fig. S1), performed without LPS-induced acute inflammation conditions to more precisely identify variations between algal conditions, a deviation of the unfixed and freshly harvested spheroids group from the control reference group was observed. This deviation is related to the moderate secretion of pro-inflammatory cytokines, and chemokines, TNF-α, IL-6, IP-10, and mKC. Once these algae were fixed with 70% ethanol, a complete re-centering around the control group was observed. A slight variation was also observed for the raw extract condition corresponding to the slight secretion of IL-6, IL-10, IL-12, mKC, and TNF-α. While the algal preservation and extract filtration were beneficial, *V. carteri* proved to be globally non-inflammatory.

## 3.3. Characterization of V. carteri living building blocks' compact stacking in saturated suspension

To build three-dimensional tissues, we relied on the compact stacking of living building blocks (LBB) formed by re-cellularized *V. carteri* (Fig. 3.A). A saturated spheroids suspension fixed in 70% ethanol, rehydrated, and primed in culture medium served as starting material in order to generate this stacking. Once obtained, spheroids needed to be characterized to visualize the morphology of such non-conventional scaffolding and check its stability when maintained under *in vitro* culture conditions.

The diameter distribution of the spheroids within this suspension was established by microscopic observation (Fig. 3.B). A normal distribution centred between 200 and 250 µm, accounting for 25% of spheroids, was observed. 70% of the spheroids ranged from 150 to 300 µm in diameter. The initial removal with a mesh of undesirable algae, which could clog the culture insert pores, was shown to be effective since spheroids with a diameter of less than 100 µm only represented only 2.70% of the whole. The saturated suspension of re-cellularized algae exhibited a density of about 74.8 $10^3$ LBB/mL, covering a developed surface area per 12-well insert of about 65 cm², thus multiplying the available surface area to about 72 times the initial insert surface.

To investigate the impact of *in vitro* culture on *V. carteri* spheroids' morphology, the algal suspension was maintained in standard insert culture conditions at 37°C and 5% CO2 with regular basal medium changes for 21 days (Fig. 3.C). From D2, the algal spheroids were closely spaced, but gaps were present at their intersection. The spheroids' spacing was progressively reduced through the draining of the excess culture medium from the apical compartment between D7 and D21. The spheroids gradually also deformed without any rupture, adopting hexagonal to square shapes due to the mechanical constraint of the sphere compact stacking. At 21 days of culture, a significant deformation was notable, the circularity of the algae having decreased significantly from 0.97 at D2 to 0.92 on completion of the culture. The algal suspension thus demonstrated a high capacity for compact incremental stacking and stability *in vitro* while retaining a degree of malleability resulting from its high deformability, thus allowing the provision of a large growth surface area with full interconnectivity.

## 3.4. Characterization of the cell adhesive properties of V. carteri

When seeded together with fixed *V. carteri* spheroids on an anti-adhesive surface, various cell types developed differing behaviors (Fig. 3.D). First, phase contrast and scanning electron microscopy observations revealed that L929 murine fibroblasts had significant cell adhesion capabilities to the algal surface. In contrast, human dermal fibroblasts (HDFn) tended to organize into spherical cell aggregates before adhering to the algal surface without covering it. Finally, human umbilical vein endothelial cells showed an intermediate behavior in that cells remained individualized, forming small chains, and some cells adhered to the algal surface without completely encircling it.

To evidence the microalga's cell adhesion properties, cell adhesion assays were performed on *V. carteri* extract-coated anti-adhesive surface in regards to non-coated anti-adhesive and cell-treated adhesive surfaces. The confluence status of HDFn and HUVEC cell types was determined following a 48-hr incubation and expressed as a ratio of the culture treated condition in Fig. 3.E. A confluency drop was observed for each cell type on the anti-adhesive condition, while the raw extract pre-treated condition exhibited significantly increased confluency. More specifically, for the HDFn, the confluency decreased to 41.3 ± 8.4% in the anti-adhesive and recovered to 73.8 ± 13.8% with the algal coating. This effect was reproduced for HUVEC, increasing from 8.7 ± 3.0% to 53.9 ± 10.7% of maximal confluency. This led us to infer that some components of *V. carteri* raw extract, presumably glycoproteins and glycans, promote cell adhesion for both human mesenchymal and endothelial cells.

## 3.5. Algal and human ECM proteic sequence homology prospective analysis

The Eukaryotic Ortholog Groups (KOG) database, which phylogenetically classifies proteins encoded by complete eukaryotic genomes, has been recently supplemented with the protein sequences deduced from the *V. carteri* genome [23]. The computer classification resulting from this entry (Fig. 4) highlighted the presence in this alga of orthologs likely to shed light on our observations concerning cell adhesion. As possible cell adhesion ligands diffusing or being exposed at the algal surface, predicted extracellular

structures of interest were found within the cellular processes and signalling category. These proteins are involved in glycoprotein modification (e.g., exostosin 1 and 2), extracellular matrix building (e.g., collagen IV and XVIII and laminin alpha and gamma), cell adhesion (e.g., teneurin), and protein interactions (e.g. von Willebrand factor).

While pherophorins represent the only extracellular matrix proteins that have been at least partially characterized experimentally and are thought to be the matrix's main constituent, only three predicted proteins (Volca2_1|8156, 9651, and 1961) enriched in proline amino acids showed slightly significant homologies ($10^{-50} \leq$ E-value $< 10^{-02}$) or identities (E-value $< 10^{-50}$) of sequences with pherophorins. Three additional protein sequences (e.g., Volca2_1|353, 10809, and 14504) indicated strong sequence homologies with a considerable number of human collagens (e.g., COL I, II, IV, and VI). A rhythmicity of G-X-Y patterns were found in these sequences, suggesting a structural homology with collagen via a triple helix motif with an additional RGD motif that could engage integrin binding. Six predicted proteins (e.g., Volca2_1|5511, 10243, and 11791) confirmed sequence homologies to one or more human laminin subunits α, β, or γ. Although the synthesis of such proteins has yet to be identified experimentally, it nevertheless highlights *V. carteri*'s potential provision of a primitive and complex extracellular matrix within and on the colony's surface, which could be structurally supported by a pherophorin-rich content clustered with cell adhesive proteins that may represent a human basal membrane and ECM-like environment.

# 3.6. Characterization of the stiffness of V. carteri spheroids

To accurately define the mechanical properties of the algal suspension at the cell level, the nanoscopic stiffness of rehydrated 70% ethanol-fixed spheroids was assessed using nanoindentation. The load generated upon a 15 000 nm indentation at a speed of 3 nm/s was quantified using a 28 µm diameter colloidal probe arranged on a rigid 0.48 N/m cantilever. Simultaneously, the spheroids diameter was measured (n = 95). The load increased with indentation. The Young modulus was determined as the slope of the linear part of the curve between 1 µm and 3 µm, considering Hertz's sphere-sphere contact model. Young's moduli as a function of the diameter of the spheroids are plotted on Fig. S2. Young's moduli ranging from 1.5 to 4 kPa for diameters ranging from 100 to 400 µm were obtained. The average Young's modulus of *V. carteri* spheroids was 2.8 ± 0.5 kPa. The diameter of the spheroids did not seem to affect their mechanical properties, as no correlation was observed between *V. carteri* spheroids' Young's modulus and diameter (Pearson's correlation test; Pearson's r = 0.063).

1. **In vitro self-assembly and in vivo biocompatibility of V. carteri-based living building blocks evaluation: the example of neonatal human dermal fibroblasts-based modular microtissue**

Morphological, proliferation, and histological studies were performed using HDFn-seeded *V. carteri* to assess macrotissue formation feasibility and its ultimate use as a soft-tissue filler.

We demonstrated that HDFn adhered to the surface of the microalga in the form of sphere-shaped aggregates, whereas when grown in 2D, HDFn expands in a fusiform manner, developing focal adhesions

and filopodia. HDFn mitochondrial activity was quantified using MTS testing and appeared to increase throughout the culture. This activity was multiplied by 4.5 between days 2 and 21, going from 0.29 to 1.31. This rise in activity was associated with the densification of fibroblast-based tissue structures at the periphery of the spheroids, highlighted by white arrows in Fig. 5.A, demonstrating HDFn proliferation. Upon 21-day culture completion, a macrotissue with integrity, although flexible and fragile, was obtained. While cultured on the surface of *V. carteri* spheroids, HDFn also exhibited alkaline phosphatase activity starting at day 2, whereas no enzymatic activity was detected when spread onto a 2D culture surface (Fig. 5.B). More and more fibroblasts were found to be positive for alkaline phosphatase expression as cells proliferated.

A fluorescent rhodamine coupled *V. carteri* suspension was used jointly to the LBB self-assembly approach (Fig. 5.C) and showed a homogeneous distribution of fibroblasts within the whole tissue thickness. However distorted, the algal spheroids remained complete and still offered a surface on which the fibroblasts expanded. Cellular clusters were formed in the cavities resulting from the stacking of multiple LBB's. Upon HES staining, this organization was recovered, and the integrity of the algal morphology, in bright pink, was observed. Its mucosal content was discernible as a thin, pale pink to yellow veil. Finally, self-organized cell sheets and clusters, whose nuclei were coloured purple and supported by a fibrous extracellular matrix, were seen in light pink to yellow.

To ascertain the *in vivo* behaviour of the HDFn-seeded *V. carteri*-based macrotissue and the resulting body response, subcutaneous implantation in athymic mice was realized. The 3D macrotissue was collected in a syringe due to its brittleness and a gelatinous suspension volume of about 150 $mm^3$ was injected on the backs of mice, creating an externally visible protruding implant. This expanded volume, indicated by an arrow in Fig. 5.E, remained detectable and unchanged in size and shape for the entire experiment duration. A bovine collagen gel injection was used as a comparison to mimic an equivalent augmentation as a control condition. Animals were euthanized at both 1 and 2 months post-implantation. Necropsy and histological analysis of the biopsies were performed. Although the same material amount was initially injected, the bovine collagen control mostly disappeared as expected, leaving only a small, barely detectable mass under the mouse skin at 1 month post-implantation (data not shown). In contrast, the HDFn-seeded *V. carteri*-based implant exhibited a large mesenchymal tissue-like structure penetrated by the surrounding blood vessels on both 1-month and 2-month post-implantation necropsies, demonstrating the great *in vivo* stability of the remodelled tissue construct. The homogeneously cellularized fibrous tissue showed, upon HE staining, remnants of spherical structures attributable to the breakdown of *V. carteri* spheroids. Histological analyses of the injected HDFn-seeded *V. carteri* biopsy specimens showed the augmentation of this thick mesenchymal tissue and the surrounding tissues without any inflammation evidence one month after implantation (i.e., absence of eosinophils, neutrophils, macrophages, or other remaining inflammatory cells). Thus, tissue remodeling and vascularization demonstrate unmistakable colonization of the implant's interstitial spaces subsequent to stromal growth. A non-cell-seeded *V. carteri*-based implant also developed a substantial mesenchymal tissue-like structure (Fig. 6. D.), which will be detailled below.

## 3.8. Evaluation of *V. carteri*'s *in vitro* influence on stem cell phenotypic fate

Both human mesenchymal and murine embryonic stem cells were seeded onto our *V. carteri*-based LBB system and cultured for up to 21 days without any adipogenic-inducing supplementation. Cell morphology and engagement in the adipogenic pathway were monitored by staining their lipid content with Oil Red O, respectively, counterstained with hemalun, or counter-labelled with DAPI and phalloidin for the observation of their cell nucleus and actin cytoskeleton either by optic or confocal microscopy.

As seen in Fig. 6.A, human adipose tissue-derived mesenchymal stem cells (hASC) were able to adhere, spread, and partially cover the surface of the algal spheroids, developing membrane protrusions similar to those exhibited when cultured in 2D. While remaining adherent and in clusters on the surface of *V. carteri* spheroids, some hASC became rounder within 48 hrs, diverting from mesenchymal cells' characteristic morphology, as shown by the condensation of their actin cytoskeleton around their nucleus (Fig. 6.B). The formation of dozens of lipids microdroplets of 1 to 3 µm in diameter, typical of adipogenic pathway drift, was observed in their cytoplasm. hASC also polarized themselves, drawing their nuclei closer to the cell membrane, and concentrating the lipid droplets in a central position, an advanced adipocytic maturation indicator. The roundness of the cell nucleus also seemed altered. As hASC differentiated rapidly, we wondered how far the adipogenic differentiation could get by pursuing the culture. The appearance and maintenance of micrometric lipid droplets in hASC cultured in 3D on the *V. carteri*-based LBB system for up to 21 days confirmed the adipogenic differentiation of the stem cells (Fig. S3). The size of each lipid droplet did not change considerably between D2 and D21. However, the increase in volume of nascent preadipocytes was correlated with the increase in the number of lipid droplets, reflecting an overall increase in the lipid content of the tissues.

To ensure the replicability of the effect observed with hASCs while broadening the pluripotency of the cells used, we aimed to apply our culture system to C3H/10T1/2 murine embryonic stem cells. C3H/10T1/2 were noted to adhere to the surface of *V. carteri* spheroids as cell aggregates (data not shown), and showed lipid microdroplet formation of about 1 µm in diameter as early as 48 hrs, demonstrating once again the *in vitro* adipogenic effect of *V. carteri* substrate. While no significant increase in C3H/10T1/2 cell size was observed, their lipid droplets significantly expanded as the culture progressed. Lipid droplets with growing diameters could be identified at 7, 14, and 21 days of culture, respectively (Fig. 6.C). While mainly maintaining anchorage points at the colony surface, some C3H/10T1/2 cells were found to be fully round, which, together with the lipid droplet presence, demonstrate their adipocyte differentiation.

## 3.9. Evaluation of *V. carteri*'s *in vivo* influence on stem cell phenotypic fate

Given the efficiency of *V. carteri* suspension to induce histogenesis and influence cellular behavior *in vitro*, we sought to explore the potential of an injectable composed exclusively of a suspension of rehydrated

70% ethanol-fixed *V. carteri* spheroids. Such a suspension was thus injected subcutaneously into an athymic mouse model. A significant reduction in the injection volume in the first few days following implantation was observed. This reduction was mainly related to the drainage of residual fluid and the reconfiguration of the algal sphere packing, as the injectable was noted to still comport a 44% V/V buffer. The overall appearance and histopathological analysis of the integrated implant provided in Fig. 6.D - did not show any particular dispersion of *V. carteri* spheroids throughout the tissues, as both closely spaced injection spots remained distinct throughout the implantation. While considering only the solid fraction, a 3.5- to 4-fold reduction in implant volume was noted. Yet, a remodelled translucent tissue structure remained visible while no inflammation-related clinical signs (i.e., redness, swelling) were detected.

The anatomopathological study showed the substitution of the *V. carteri* suspension by a mesenchyme-like tissue. This 500-µm-thick remodelled tissue presented a homogeneous extracellular matrix, cellular infiltration, and integration into a fibrous capsule structurally similar to the interstitial connective tissue overlaid with standard tissue layers of epidermis, dermis, dermal white adipose tissue, and the panniculus carnosus without visible alteration or algal infiltration. Athymic mice are covered only with reduced-size "aborted" hairs [24] but still display numerous hair follicles, integrating associated structures such as sebaceous glands and stem cell bulges. No vascular structures could be identified within the remodelled tissue. However, blood vessels were found in the surrounding interstitial tissue, strongly suggesting that the remodelled tissue may be infiltrated and supplied by non-observable capillary systems. The neoextracellular matrix showed no remaining algal structures but comprised numerous foamy macrophages and fibroblasts, indicating that material degradation and matrix remodelling could still be ongoing under mild inflammatory conditions. Interestingly, in all grafted animals, mesenchymal tissue displayed niches of about ten growing adipocytes distributed throughout the implant, particularly in its lower part.

# 4. Discussion

# 4.1 An alternative support of vegetal origin for animal cell culture

Tissue engineering strategies are generally directed towards the molecular, structural and mechanical reproduction of tissue microenvironments *in vivo*, researching cell adhesion, migration, proliferation and differentiation, as well as ECM synthesis and remodelling, to initiate, regulate and guide the regeneration process (15). Materials derived from animal ECM, as natural components of tissues, are generally preferred for the formation of scaffolds, in which they participate both as structural elements and to provide the appropriate cellular niche. Yet their use still raises challenges to sustainably promote tissue regeneration (i.e., matrix variability, tuneable complexity, poor mechanical properties, high degradability, and variable immunological response) (16). This observation has prompted researchers to take other paths and to explore, for example, different pre-existing systems, even apparently distant from animal organization, but all having support structures likely to be more correctly tolerated because of their

biological character, while respecting the objective of an organization as close as possible to the tissue of origin. *V. carteri* seems a good candidate in this perspective. Thus, on non-adherent surfaces, the addition of a coating composed of *V. carteri* cell extract significantly increased the cell adhesion of human fibroblasts and endothelial cells. Furthermore, murine and human cells of mesenchymal and endothelial origin were capable of developing cell adhesion to the surface of decellularized - that is, stripped of their outer plant cell layer - algae. Although the cells used adopted variable adhesion strategies, all adhered well to the proposed support, demonstrating the great potential of *V. carteri* as a cell vector. The exact nature of the different molecular elements that participate in the underlying architecture of the spheres of *V. carteri* is not completely elucidated and remains to be investigated. However, some molecules already identified have characteristics that arouse interest.

Among these, the glycoproteins known as pherophorins (Ph) hold a special place. Pherophorins are predominant in the composition of *V. carteri*, contained and specific to each algal compartment from the cell walls, inner membranes to ECM meshes (17, 18). Following complete genome sequencing of *V. carteri* (19), 49 potential pherophorin-like protein sequences have been identified by genetic analysis. However, to our knowledge, only seven have been examined experimentally, mainly for developmental biology purposes (12, 20, 21, 22). As hydroxyproline-rich glycoproteins (HRGPs) with Ser((hydroxy-)Pro)n repeats in the centred HR domains, pherophorins are classified as extensins. They also contain saccharide-binding specificities in their A and B side domains, a feature present in lectins as well (23). These molecular specificities allow self-assembly and autocatalytic crosslinking, producing an insoluble fibrous network, as observed e.g. for the DZ1 and DZ2 pherophorins of the deep zone (12). As crosslinking proteins, they may be considered functionally analogous to animal collagen in the building of ECM architectures (13). The predominance of hydroxyprolines in their respective protein sequences largely contributes to this view. Indeed, in higher eukaryotes, hydroxyproline is an essential compound of fibrillar collagens, where it represents 14% of the total amount of imino and amino acids. Moreover, in addition to the structural maintenance of the collagen I triple helix (24, 25), proline hydroxylation has been shown to be essential for the binding, stabilization and subsequent cell adhesion of integrins (26). Pherophorin I and II, two cellular zone pherophorins of *V. carteri* contain 10.75% and 7.72% proline respectively, all potential target for hydroxylation. Interestingly, the SSG185 protein, also isolated from the cellular zone, harbours a very high hydroxyproline content (19.17%) and has been classified recently as a pherophorin as well (27), Pherophorin S, the major component of the deep zone, peaks at 18.19% proline residues, most of them if not all being hydroxylated. In some portions of the Pherophorin S and SSG185 sequence, the hydroxyprolines are not scattered but organized into a long, nearly unbroken consecutive sequence. This characteristic is found in an exacerbated way in the DZ-HRGP protein, another protein also produced in the deep zone in response to sex pheromones and wounds, which is almost exclusively composed of hydroxyprolines (28). Such a consecutive arrangement is characteristic of a very marked polyproline helix (PPII) structural organization (29). This type of helix is considered as relatively stiff (30) and very probably contributes to the overall mechanical properties of the *V. carteri* sphere (see below).

Hydroxyproline residues are the main target of O-glycosylation in plants. In the plant kingdom, this post-translational modification is initiated by the addition of Galactose and/or Arabinose and then further

extended with complex poly-Arabinose or branched Galactose chains. Serine residues adjacent to hydroxyproline glycosites may also be glycosylated (31). Because of their high hydroxyproline content, plant HRGPs are thus highly O-glycosylated and have been considered functionally equivalent to mammalian proteoglycans such as mucins (32). Mucins are large, heavily glycosylated proteins that are the main constituent of many mucus and which play important physiological roles in cell signalling, immune response, and cell adhesion (33). Although the O-glycosylation of microalgae proteins is still poorly deciphered (34), the glycosylation profiles of HRGPs from *V. carteri* seem quite similar to the profiles observed in plants, with long glycosylated chains, mostly made up of arabinose and galactose subunits (12, 20, 21) which can also include mannose and glucose sub-units, as does the ISG glycoprotein (35). Crosslinking of saccharides with phosphodiester bridges between arabinose residues, and in a single case, the additional attachment of a highly sulfated arabinomannan have been moreover observed (36). The ConA lectin, that specifically binds α-mannose/α-glucose on N-glycans with little cross-reactivity (37, 38) enabled us to visualize the involvement of these sugars in the general architecture of *V. carteri* and more generally highlighted the importance of O-glycosylation in the cohesion of the alga. Since the labelling also revealed the marked presence of highly glycosylated proteins on the surface of the algal spheres, we hypothesize that the glycosylated HRGPs present in the cell layer of *V. carteri* may also play an adhesive role, close to that played by mucins, when they are brought into contact with cells, whatever their origin. All our observations strongly suggest the existence of a *V. carteri*-specific organization in which pherophorins and other potentially associated HRGPs, all with a high hydroxyproline content and a high degree of O-glycosylation, play by their interactions both a collagen-like structural role and an mucin-like adhesive role.

KOG genome annotation and protein sequence comparison using BlastP enabled us to identify other proteins of interest that could contribute to the algal sphere properties. These proteins show sequence similarities with essential proteins of the human ECM and are also likely to contribute to the cellular adhesive properties of *V. carteri*. For example, three additional protein sequences were found to show direct similarities to human collagens, through the presence of the characteristic G-X-Y rhythmicity in their amino acid sequence (39). The existence in their sequence of an additional RGD motif suggests also a possible integrin binding (40). Six predicted proteins confirmed moreover sequence similarities with one or more of the human laminin subunits. Laminins are glycoproteins that constitute one of the major components of the basal lamina of eukaryotic cells, where they play an active role in cell differentiation and adhesion (41). Although the synthesis of all these proteins has not yet been identified experimentally, the possible joint presence of laminin alongside with pherophorins and collagens sheds light on what could constitute a basic architecture of an entirely credible animal-compatible ECM. It in fact supposes the possibility in *V. carteri* of the existence of a complex primitive extracellular matrix inside and on the surface of the colony. This matrix could be structurally built on the richness in HRGP, associated with cell adhesion proteins. The whole would thus form a hosting structure which efficiently facilitates cell implantation and proving to be as effective, if not more, than a matrix artificially reconstituted *in vitro* from independent elements.

# 4.2 Algal properties enabling tissue engineering and soft tissue reconstruction

The algae suspension is composed of microspheres normally distributed around 250 µm in diameter. When each of the spheres is covered with cells, it forms stackable cell blocks. This individual block stacking organization provides infinite malleability for multi-volume shaping. It also has a considerably increased adhesion surface compared to a flat or even porous material. The variability of carrier sphere sizes allows for greater compaction while creating niches at their intersections and an interstitial continuum, ensuring complete interconnectivity. In the case of conventional scaffolds, ensuring efficient mass transport allowing easy diffusion of nutrients and gases is very difficult because the solid phase of the material too often acts as a barrier (42). Throughout the compaction of the spheres, this diffusion is significantly decreased between D0 and D2, since studies of the diffusion coefficient in random packing of polydispersed hard spheres have shown that the effective diffusion was mainly decreased with the increase in the volume fraction solid (43). In other words, the progressive reduction of the interstitial void between the spheres due to cell growth slows the diffusive transport. However, the high density which results from this internal compaction and the progressive deformation, without immediate rupture, of the algal spheres during the culture time are favourable to an increase in the cohesion of the tissue structure created. When implanted, seeded collagen matrices generally present a strong degradability, which affects the stability *in vivo* but facilitates the integration *in situ*. However, although the *in vivo* resorption rate of a collagen implant can be regulated by controlling its density and degree of intermolecular cross-linking (44), it tends to generate a foreign body response (45). When we injected a suspension of rehydrated 70% ethanol-fixed *V. carteri* spheres without any cell seeded, we noticed an absence of dispersion of the spheres throughout the tissues. One month after injection, the sphere appeared resorbed and substituted by a mesenchyme-like tissue. The experience was reproduced using agglomerated human-cell-seeded blocks. Once this *V. carteri*-based compact tissue was obtained and subcutaneously implanted, we could observe that it remained stable, highly cellularized and vascularized up to 2 months after implantation. Again, the alga had almost disappeared. Since no significant inflammation was observed during the degradation of *V. carteri* in different implantation conditions, the algal support may have been degraded *in vivo* by a fibroblast-dependent phagocytic mechanism related to matrix homeostatic remodelling (46). More investigations have however to be conducted to evaluate tissue ingrowth and remodelling within the implant, particularly by distinguishing the respective contribution of murine and human fibroblasts to the final tissue obtained.

Biomaterials are not only passive carriers but are also designed to utilize the mechanobiology of seeded cells to promote their differentiation, a process that is more difficult to achieve in hormone-induced 2D cultures. For example, hASCs can differentiate into neurons, adipocytes, myoblasts, or osteoblasts when grown on substrates with stiffnesses measured by their Young's modulus of 0–1, 2–4, 8–10, and > 30 kPa, respectively (16, 47, 48). However, in the case of adipose tissues, most engineered materials demonstrate a Young modulus that is significantly higher ($E \approx 1$ MPa) than the soft tissue they aim at reproducing (1–10 kPa). Indeed, the Young’s modulus of fibrillar proteins, which often make up these

materials, is much greater than that of tissue component assemblies, which in turn are significantly stiffer than the elastic properties of bulk tissue samples (49). As demonstrated in the case of obesity, ECM stiffness increases impaired adipogenesis by blunting the sensitivity to insulin and lipolytic cues, as well as the secretion of adipokines (50). *V. carteri* provides a spherical substrate with an overall stiffness of about 3 kPa that is stable regardless of colony diameter or stage of development, demonstrating the homogeneity of the suspension's mechanical properties. It is close to adipocyte-to-adipose tissue like-stiffness (51, 52) and fully fits within the 2–4 kPa range of estimated optimal stiffness for adipogenesis mechanical induction. As mentioned above, this ideal situation can be attributed to the high amount of hydroxylated proline conferred by the predominance of pherophorins and other HRGPs in the ECM of *V. carteri*. Proline hydroxylation has been shown to improve collagen elasticity (53). The hyperglycosylation of these same residues also contributes to this overall flexibility. On the other hand, the rigid modules of the polyproline helices present in some HRGPs have an antagonistic effect since they maintain a certain stiffness. It seems that the mechanical properties of the spheres of *V. carteri* result from a balance between these two phenomena. It has been previously shown that *in vitro* recreation of adipose rigidity can stimulate the adipogenesis of human adipose-derived mesenchymal stem cells without the use of chemical media additives (54) and some explanations have been proposed to this phenomenon. Mesenchymal stem cells cultured on flexible substrates significantly reduce their cell surface area and aspect ratio as a result of low cytoskeleton contractility (55), influencing adipocyte differentiation via ERK signalling (56), promoting upregulation of gene expression of all three adipogenic markers (i.e., PPARγ, CEBPα, and aP2), and lipid accumulation (54). The actin cytoskeleton reorganization dynamics also affect the roundness of the nucleus during adipocyte differentiation (57). In addition to adipocyte stiffness adequacy, *V. carteri* colony sphericity may also foster adipogenesis. Indeed, the cellular geometry driven by cellular contractility influences MSC differentiation: cells in rounder shapes that promote low contractility are preferred to follow an adipocyte lineage, while cells in elongated shapes promote increased myosin contractility, which enhances pathways associated with osteogenesis (55). Adipocytes' static strain on neighbouring preadipocytes promotes differentiation (58, 59). Whatever its origin, *V. carteri* mechanical mimicry with adipose tissue is able to induce adipocytic differentiation of mesenchymal stem cells very efficiently.

## 4.3 Durable, implantable, biocompatible and non-inflammatory building blocks

The microalga was found to be in general physically stable under culture conditions and cytocompatible against ISO 10993-5 standards, maintaining high levels of cell viability in the murine fibroblast cell line L929. As a balanced inflammation (i.e., not excessive in its intensity and duration) stimulates tissue renewal allowing the formation or remodeling of tissues, the inflammatory and immunogenic potential of *V. carteri* was evaluated *in vitro* by determination of J774.2 murine macrophages secretome under exposure. These experiments showed the absence of a global pro-inflammatory response, indicating macrophage non-activation at 48 h of exposure and non-pro-inflammatory and non-immunogenic resulting properties. Only exposure to living algae generated a weak pro-inflammatory response that could be induced by toxins synthesized upon either or both algal stress and mortality. Schenck et al. (60)

observed no significant inflammatory response to *C. reinhardtii*, V. *carteri*-related unicellular algae, when implanted in both athymic nude mice and zebrafish *in vivo* models. This photosynthetic graft also demonstrated that *C. reinhardtii* in the implanted scaffolds did not trigger any deleterious local or systemic immune responses in a 90-days follow-up, allowing full tissue regeneration in humans (61). *V. carteri*'s anti-inflammatory effect of the algae could be further investigated, upon LPS-activation for instance, as a decrease in proinflammatory IL-9 and IL-15 were observed for all algal treated conditions. Green algae phytochemicals such as hydroxylated fatty acids, chlorophyll-derived pheophorbides, carotenoids, and glycoglycerolipids showed anti-inflammatory effects by decreasing nitric oxide intracellular levels (62, 63). Respectively used as dry biomass or extracts, *C. debaryana*, and *P. japonica* have demonstrated their anti-inflammatory efficacy in the treatment of intestinal mucosa inflammation *in vivo* (64, 65). Given the phylogenetic proximity of *C. reinhardtii* and *V. carteri*, which are both used as inactivated materials, this allows for great confidence in the overall biocompatibility of the algae.

When cells (HDFn) were cultivated at the surface of *V. carteri* beads, the cells expressed alkaline phosphatase (AP) activity exclusively when grown in 3D. The expression began at D2 and lasting until D21. As a high level of AP correlates with pluripotency and undifferentiated pluripotent stem cell phenotypes (66), *V. carteri* could induce fibroblast dedifferentiation, forming fibroblast aggregates, and confining them into specific environments. Indeed, mechanically confined fibroblasts have shown the ability to reprogram stem cell-like cells and rejuvenate, demonstrating phosphatase alkaline activity (67). Yet, while high AP is associated with pluripotency, AP is also ubiquitous and known to be actively produced in bone, liver, and kidney (68). To validate this statement, additional research should be conducted, including the determination of pluripotency transcription factors' expression in HDFn seeded on *V. carteri*. Moreover, because fibroblasts are contractile cells and *V. carteri* exhibits signs of deformability, these cells have been able to manage this interstitial volume drain by substituting it with extracellular matrix while proliferating, as demonstrated by the increase in mitochondrial activity and histological analysis of ECM neosynthesis. Altogether, our LBB' compact stacking system was found suitable to build structured tissue showing an even distribution of cells and matrix secretion over the whole thickness of the created tissue. According to our *in vitro* results, cellularised *V. carteri* living building blocks seems fitted for the construction of three-dimensional tissues.

# 4.4 Differenciation orientation and neogenesis

In the search for alternative tissue engineering approaches, many researchers have now overcome the daunting task of crossing the kingdoms and focus on microalgae and plant-based materials. By taking advantage of similarities in the vascular structure of plant and animal tissues, Gershlak et al. (69) were able to use a decellularized plant tissue as a vascularized scaffold for tissue engineering applications. Moreover, the incorporation of *Spirulina* in electrospun scaffolds has demonstrated improvement in cytocompatibility by providing a wide range of vital nutrients to the cells, thereby affecting their metabolism (70). Similarly, living photosynthetic *C. reinhardtii* volvocine algae implanted in a wound defect effectively delivered oxygen in situ to limit hypoxia and promote wound healing (60, 61). Here, we aimed to take advantage of *V. carteri*'s global structure and collagen-like ECM for soft tissue

augmentation. Conversely, to the collagen matrix based reconstructed tissues, *V. carteri*-based mesenchymal tissue remained stable, highly cellularized, and vascularized for up to 2 months post-implantation. Since no significant inflammation was observed during the degradation of *V. carteri* in these implantation conditions the alga may have been degraded *in vivo* by a fibroblast-dependent phagocytic mechanism related to matrix homeostatic remodelling (46).

Adipose tissue engineering has recently emerged as a growing field in regenerative medicine (71). Unfortunately, the biomaterials currently available for adipose tissue substitution still face limitations in guaranteeing long-term tissue regeneration. Natural constituents, being mostly extracellular matrix elements, are sensitive to remodelling. In contrast, synthetic materials display better volume preservation but lack the naturalness to produce structural and functional soft tissue regeneration. Such material usually generates a foreign body response, stabilizing and isolating the volume from the rest of the body via fibrous tissue encapsulation (54, 72). Recently, research efforts have focused on the design of bioactive materials that would target specific regenerative mechanisms (15). *In vitro* adipogenesis, aiming to differentiate mesenchymal stem cells into preadipocytes with the ultimate goal of producing mature adipocytes, is commonly induced with dexamethasone (DEX), isobutylmethylxanthine (IBMX), and insulin. These chemicals trigger a series of transcription factors, including CREBP, KLF4, 5, and 9, CEBPβ, and δ that will subsequently activate the second wave of adipogenic gene inducers, PPARγ, CEBPα, and SREBP (73). The duration, degree, and type of adipogenic differentiation achieved differ according to the cell type (i.e., stem cell origin, primary pre-adipocyte) and the composition of the induction cocktail. Differentiation protocols generally require about 10 days of culture without ultimately reaching the unilocular white adipocyte stage in 2D culture (51, 74).

*V. carteri* living building blocks-mediated culture generated massive lipid droplet synthesis and maintenance in culture duration on both C3H/10T1/2 and hASC, undeniably demonstrating the capabilities of the alga as a material to promote adipogenesis without any addition of induction factors. hASC exhibited both cytoskeleton anisotropy as well as nucleus polarization and roundness alteration as early as 48 h, reflecting a significant shift towards the adipogenic pathway (51, 75). By contrast, 2D adipogenic differentiation of both C3H/10T1/2 and hASC would necessitate 7–10 additional days of culture post-confluency in an adipogenic induction medium including at least insulin and thiazolidinedione-insulin sensitizers (76, 77). While the number of microdroplets per cell for hASC increased as the culture progressed, no significant growth in lipid microdroplet size was observed. On the contrary, a distinct lipid microdroplet expansion could be observed for C3H/10T1/2. This differentiation limit can be explained by interspecies differences in their lipid accumulation mechanisms, especially those regulated by PPARγ. Human adipose cells, unlike mouse adipose cells, cannot secrete endogenous PPARγ ligands *in vitro*, necessitating the addition of PPARγ agonist supplementation (78). To achieve advanced adipocyte differentiation, *in vitro* exogenous sources of PPARγ ligands could be added by supplementation in the medium or by establishing co-culture with PPARγ ligands-secreting cells such as human adipose tissue-derived microvascular endothelial cells (79). To further assess the level and nature of the adipocyte differentiation induced by *V. carteri*-living building blocks-mediated culture, the expression levels of adipogenic genes, transcription factors, adipokines (e.g., adiponectin, leptin), as well

as lipoprotein lipase secretion levels, could be quantified. Moreover, type-specific and advancement-specific differentiation markers could be screened by immunostaining.

# Conclusion

Data presented here demonstrate the potential of *V. carteri* as an innovative alternative structuring biomaterial for soft-tissue engineering. By providing a hypothesized basal-membrane-like environment and developing sequence similarities with mammalian ECM elements such as collagen and laminin subunits, the alga exhibited capabilities in sustaining cell adhesion and supporting histogenesis both *in vitro* and *in vivo*. The compact packing of algal-based cell-seeded spheroids (LBBs) offers an extensive, unique, and integrally interconnected culture surface suitable for cellularization and diffusion throughout the template. Modulating cellular guidance, containment, and heterogeneity, the *V. carteri*-based substrate represents an innovative matrix of vegetal origin for such uses, allowing adhesion, proliferation, and matrix secretion with potential differentiation properties. This work is a proof of concept of the feasibility of a modular approach for cell-seeded *V. carteri* living building blocks for three-dimensional tissue formation and their use in *in vivo* soft tissue regeneration. We demonstrated *V. carteri*'s adipogenic effects both *in vitro* and *in vivo*. The adipogenesis-driving properties of these structures may well be directly tied to the capability of the alga to mimic adipose tissue structurally, mechanically, and molecularly, as a provision of fundamental biochemical signals of extracellular matrix, cell adhesion, and lipid accumulation is suspected.

# Abbreviations

extracellular matrix (ECM); living building blocks (LBB); Dulbecco's modified eagle's medium (DMEM); Fetal Bovine Serum (FBS); Human Dermal Fibroblasts (HDFn); Human Umbilical Vein Endothelial Cells (HUVEC); Human adipose-derived mesenchymal stem cells (hASC); Mesenchymal Stem Cell (MSC); hematoxylin-eosin (HE); hematoxylin-eosin safran (HES); dexamethasone (DEX); isobutylmethylxanthine (IBMX);

# Declarations

Ethics approval and consent to participate: n/a

Consent for publication: n/a

Availability of data and materials:

Data will be made available on request.

Competing interests:

The authors declare that they have no known competing financial interests or personal relationships that could have appeared to influence the work reported in this paper.

Funding:

MS received a fellowship from the French Ministry of Science and Technology.

Authors' contributions:

Conception and design: P.V., C.O.S., C.E Data acquisition: M.S., P.V. Analysis and interpretation of data: M.S., C.O.S., C.E. Study supervision: F.D., C.O.S., C.E. Critical drafting/revision of manuscript: all authors.

Acknowledgements:

The authors thank Vanessa Bleicher- and Ulysse Peirera for technical help, the Service Analyses Physico-Chimiques (SAPC) for the imaging , and all their colleagues for helpful comments throughout this effort.

Christophe Egles thank the RIN program of the Région Normandie, Evreux Portes de Normandie and the FEDER european fund for their support.

# References

1. Ouyang L, Armstrong JPK, Salmeron-Sanchez M, Stevens MM. Assembling Living Building Blocks to Engineer Complex Tissues. Adv Funct Mater. 2020;30(26):1909009.
2. Szathmáry E, Smith JM. The major evolutionary transitions. Nature. 1995;374(6519):227–32.
3. Matt G, Umen J, Volvox. A simple algal model for embryogenesis, morphogenesis and cellular differentiation. Dev Biol. 2016;419(1):99–113.
4. Kirk DL. A twelve-step program for evolving multicellularity and a division of labor, *BioEssays*,(2005) vol. 27(3), p. 299–310.
5. Herron MD, Michod RE. Evolution of complexity in the volvocine algae: transitions in individuality through darwin's eye. Evolution. 2008;62(2):436–51.
6. de Maleprade H, Moisy F, Ishikawa T, Goldstein RE. Motility and phototaxis of *Gonium*, the simplest differentiated colonial alga. Phys Rev E. 2020;101(2):022416.
7. Smith GM. A Comparative Study of the Species of Volvox. Trans Am Microsc Soc. 1944;63(4):265.
8. Halder N. Two algal species of Volvox L. with their taxonomy and ecology from West Bengal, India. Songklanakarin J Sci Technol. 2016;38(4):435–7.
9. Kirk DL. Volvox: A Search for the Molecular and Genetic Origins of Multicellularity and Cellular Differentiation. Cambridge, U.K: Cambridge University Press; 1998.
10. Hallmann A. The pherophorins: common, versatile building blocks in the evolution of extracellular matrix architecture in Volvocales. Plant J. 2006;45:292–307.
11. Hallmann A, Amon P, Godl K, Heitzer M, Sumper M. Transcriptional activation by the sexual pheromone and wounding: a new gene family from Volvox encoding modular proteins with

(hydroxy)proline-rich and metalloproteinase homology domains: VMPs: inducible metalloproteinases from Volvox. Plant J. 2001;26(6):583–93.

12. Ender F, Godl K, Wenzl S, Sumper M. Evidence for Autocatalytic Cross-Linking of Hydroxyproline-Rich Glycoproteins during Extracellular Matrix Assembly in Volvox. Plant Cell. 2002;14(5):1147–60.
13. Kieliszewski MJ, Shpak E. Synthetic genes for the elucidation of glycosylation codes for arabinogalactan-proteins and other hydroxyproline-rich glycoproteins. Cell Mol Life Sci. 2001;58(10):1386–98.
14. Provasoli L, Pintner IJ. « Artificial media for fresh-water algae: problems and suggestions. », in *Ecology of Algae*, Tryon, C. A., Jr. & Hartmann R. T., University of Pittsburgh, Pittsburgh: Pymatuning Laboratory of Field Biology, (1959), p. 84–96.
15. Williams DF. Challenges with the Development of Biomaterials for Sustainable Tissue Engineering. Front Bioeng Biotechnol. 2019;7:127.
16. Aamodt JM, Grainger DW. Extracellular matrix-based biomaterial scaffolds and the host response. Biomaterials. 2016;86:68–82.
17. Sumper M, Hallmann A. Biochemistry of the Extracellular Matrix of Volvox », in *International Review of Cytology* (1998), vol. 180, Elsevier, p. 51–85.
18. Hallmann A. Extracellular Matrix and Sex-Inducing Pheromone in Volvox », in *International Review of Cytology* (2003), vol. 227, Elsevier, p. 131–182.
19. Prochnik SE, et al. Genomic Analysis of Organismal Complexity in the Multicellular Green Alga *Volvox carteri*. Science. 2010;329(5988):223–6.
20. von der Heyde B, Hallmann A. Targeted migration of pherophorin-S indicates extensive extracellular matrix dynamics in Volvox carteri. Plant J. 2020;103(6):2301–17.
21. Godl K. Differential targeting of closely related ECM glycoproteins: the pherophorin family from Volvox. EMBO J. 1997;16(1):25–34.
22. Wenzl S, Thym D, Sumper M. Development-dependent modification of the extracellular matrix by a sulphated glycoprotein in *Volvox carteri*, *EMBO J.* (1984), vol. 3, n$^{o}$ 4, p. 739–744.
23. Hallmann A. « The pherophorins: common, versatile building blocks in the evolution of extracellular matrix architecture in Volvocales ». Plant J. 2005;45(2):292–307.
24. Sakakibara S, Inouye K, Shudo K, Kishida Y, Kobayashi Y, Prockop DJ. Synthesis of (Pro-Hyp-Gly)n of defined molecular weights Evidence for the stabilization of collagen triple helix by hydroxypyroline, *Biochim. Biophys. Acta BBA - Protein Struct.* (1973), vol. 303, n$^{o}$ 1, p. 198–202.
25. Jenkins CL, Bretscher LE, Guzei IA, Raines RT. Effect of 3-Hydroxyproline Residues on Collagen Stability, *J. Am. Chem. Soc.* (2003), vol. 125, n$^{o}$ 21, p. 6422–6427.
26. Sipilä KH, et al. « Proline hydroxylation in collagen supports integrin binding by two distinct mechanisms ». J Biol Chem. 2018;293(20):7645–58.
27. von der Heyde B, Hallmann A. Targeted migration of pherophorin-S indicates extensive extracellular matrix dynamics in Volvox carteri. Plant J. 2020;103(6):2301–17.

28. Ender F, Hallmann A, Amon P, Sumper M. Response to the sexual pheromone and wounding in the green alga volvox: induction of an extracellular glycoprotein consisting almost exclusively of hydroxyproline. J Biol Chem. 1999;274(49):35023–8.
29. Adzhubei AA, Sternberg MJ, Makarov AA. Polyproline-II helix in proteins: structure and function. J Mol Biol. 2013;425(12):2100–32.
30. Wilhelm P, Lewandowski B, Trapp N, Wennemers H. A crystal structure of an oligoproline PPII-helix, at last. J Am Chem Soc. 2014;136(45):15829–32.
31. Joshi HJ, Narimatsu Y, Schjoldager KT, Tytgat HLP, Aebi M, Clausen H, Halim A. SnapShot: O-Glycosylation Pathways across Kingdoms, *Cell* (2018), vol. 172(3), p. 632–632.
32. Chaturvedi P, Singh AP, Batra SK. Structure, evolution, and biology of the MUC4 mucin. FASEB J. 2008;22(4):966–81.
33. Martínez-Sáez N, Peregrina jM, Corzana F. Principles of mucin structure: implications for the rational design of cancer vaccines derived from MUC1-glycopeptides. Chem Soc Rev. 2017;46(23):7154–75.
34. Mathieu-Rivet E, Mati-Baouche N, Walet-Balieu ML, Lerouge P, Bardor M. N- and O-Glycosylation Pathways in the Microalgae Polyphyletic Group. Front Plant Sci. 2020;11:609993.
35. Schlipfenbacher R, Wenzl S, Lottspeich F, Sumper M. An extremely hydroxyproline-rich glycoprotein is expressed in inverting *Volvox* embryos. FEBS Lett. 1986;209(1):57–62.
36. Ertl H, Mengele R, Wenzl S, Engel J, Sumper M. The extracellular matrix of Volvox carteri: molecular structure of the cellular compartment. J Cell Biol. 1989;109(6):3493–501.
37. Varki A, Esko J, Colley K. Cellular Organization of Glycosylation, in *Essentials of Glycobiology* (2009), The Consortium of Glycobiology Editors., Cold Spring Harbor (NY): Cold Spring Harbor Laboratory Press.
38. Ruiz-May E, Sørensen I, Fei Z, Zhang S, Domozych D, Rose J. The Secretome and N-Glycosylation Profiles of the Charophycean Green Alga, Penium margaritaceum, Resemble Those of Embryophytes, *Proteomes* (2018), vol. 6(2), p. 14.
39. Ricard-Blum S. The collagen family. Cold Spring Harb Perspect Biol. 2011;3(1):a004978.
40. D'Souza SE, Ginsberg MH, Plow EF. Arginyl-glycyl-aspartic acid (RGD): a cell adhesion motif. Trends Biochem Sci. 1991;16(7):246–50.
41. Timpl R, Rohde H, Robey PG, Rennard SI, Foidart JM, Martin GR. Laminin–a glycoprotein from basement membranes. J Biol Chem. 1979;254(19):9933–7.
42. Fiedler T, et al. A comparative study of oxygen diffusion in tissue engineering scaffolds. J Mater Sci Mater Med. 2014;25(11):2573–8.
43. Hlushkou D, Liasneuski H, Tallarek U, Torquato S. Effective diffusion coefficients in random packings of polydisperse hard spheres from two-point and three-point correlation functions. J Appl Phys. 2015;118(12):124901.
44. Ghanaati S, et al. Evaluation of the tissue reaction to a new bilayered collagen matrix *in vivo* and its translation to the clinic. Biomed Mater. 2011;6(1):15010.

45. Rothamel D, Schwarz F, Sager M, Herten M, Sculean A, Becker J. Biodegradation of differently cross-linked collagen membranes: an experimental study in the rat. Clin Oral Implants Res. 2005;16(3):369–78.
46. Atala A. From Tissue to Organ Engineering, in *Comprehensive Biomaterials* (2011), Elsevier, p. 547–62.
47. Tse JR, Engler AJ. Stiffness Gradients Mimicking *In Vivo* Tissue Variation Regulate Mesenchymal Stem Cell Fate. PLoS ONE. 2011;6(1):e15978.
48. Li Y et al. Application of External Force Regulates the Migration and Differentiation of Adipose-Derived Stem/Progenitor Cells by Altering Tissue Stiffness, *Tissue Eng. Part A* (2019), vol. 25, p. 1614–1622.
49. Akhtar R, Sherratt MJ, Cruickshank JK, Derby B. Characterizing the elastic properties of tissues. Mater Today. 2011;14(3):96–105.
50. Tsai Y, Huang A, Lin Y, Kao L, Tang M, Tsai P. Adipose tissue stiffness in the development of metabolic diseases. FASEB J. 2022;36:R5289. nº S1.
51. Abuhattum S, et al. Adipose cells and tissues soften with lipid accumulation while in diabetes adipose tissue stiffens. Sci Rep. 2022;12(1):10325.
52. Alkhouli N, et al. The mechanical properties of human adipose tissues and their relationships to the structure and composition of the extracellular matrix. Am J Physiol -Endocrinol Metab. 2013;305(12):E1427–35.
53. Di Medio L, Brandi ML. Advances in bone turnover markers, in *Advances in Clinical Chemistry* (2021), vol. 105, Elsevier, p. 101–140.
54. Young DA, Choi YS, Engler AJ, Christman KL. Stimulation of adipogenesis of adult adipose-derived stem cells using substrates that mimic the stiffness of adipose tissue. Biomaterials. 2013;34(34):8581–8.
55. Kilian KA, Bugarija B, Lahn BT, Mrksich M. Geometric cues for directing the differentiation of mesenchymal stem cells, *Proc. Natl. Acad. Sci.* (2010), vol. 107(11), p. 4872–4877.
56. Chen L, Hu H, Qiu W, Shi K, Kassem M. Actin depolymerization enhances adipogenic differentiation in human stromal stem cells. Stem Cell Res. 2018;29:76–83.
57. McColloch A, Rabiei M, Rabbani P, Bowling A, Cho M. Correlation between Nuclear Morphology and Adipogenic Differentiation: Application of a Combined Experimental and Computational Modeling Approach. Sci Rep. 2019;9(1):16381.
58. Shoham N, Gottlieb R, Sharabani-Yosef O, Zaretsky U, Benayahu D, Gefen A. Static mechanical stretching accelerates lipid production in 3T3-L1 adipocytes by activating the MEK signaling pathway. Am J Physiol -Cell Physiol. 2012;302(2):C429–41.
59. Shen JX, et al. 3D Adipose Tissue Culture Links the Organotypic Microenvironment to Improved Adipogenesis. Adv Sci. 2021;8(16):2100106.

60. Schenck TL, et al. Photosynthetic biomaterials: A pathway towards autotrophic tissue engineering. Acta Biomater. 2015;15:39–47.
61. Obaíd ML, et al. A First in Human Trial Implanting Microalgae Shows Safety of Photosynthetic Therapy for the Effective Treatment of Full Thickness Skin Wounds. Front Med. 2021;8:772324.
62. Manabe Y, Takii Y, Sugawara T. Siphonaxanthin, a carotenoid from green algae, suppresses advanced glycation end product-induced inflammatory responses. J Nat Med. 2020;74(1):127–34.
63. Qiu S, et al. Chemometrics-Assisted Identification of Anti-Inflammatory Compounds from the Green Alga Klebsormidium flaccidum var. zivo. Molecules. 2020;25(5):1048.
64. Ávila-Román J, et al. Preventive effect of the microalga *Chlamydomonas debaryana* on the acute phase of experimental colitis in rats. Br J Nutr. 2014;112(7):1055–64.
65. Rahmawati L, et al. Anti-Inflammatory Activities of the Ethanol Extract of Prasiola japonica, an Edible Freshwater Green Algae, and Its Various Solvent Fractions in LPS-Induced Macrophages and Carrageenan-Induced Paw Edema via the AP-1 Pathway. Molecules. 2021;27(1):194.
66. Štefková K, Procházková J, Pacherník J. Alkaline Phosphatase in Stem Cells, *Stem Cells Int.* (2015), vol. 2015, p. 1–11.
67. Roy B, Yuan L, Lee Y, Bharti A, Mitra A, Shivashankar GV. Fibroblast rejuvenation by mechanical reprogramming and redifferentiation, *Proc. Natl. Acad. Sci.* (2020), vol. 117(19), p. 10131–10141.
68. Moss DW. Alkaline phosphatase isoenzymes. Clin Chem. 1982;28(10):2007–16.
69. Gershlak JR, et al. Crossing kingdoms: Using decellularized plants as perfusable tissue engineering scaffolds. Biomaterials. 2017;125:13–22.
70. Steffens D, et al. A New Biomaterial of Nanofibers with the Microalga *Spirulina* as Scaffolds to Cultivate with Stem Cells for Use in Tissue Engineering. J Biomed Nanotechnol. 2013;9(4):710–8.
71. Mughal M, Sindali k, Man J, Roblin P. Fat chance': a review of adipose tissue engineering and its role in plastic and reconstructive surgery. Ann R Coll Surg Engl. 2021;103(4):245–9.
72. Lemperle G, Morhenn V, Charrier U. Human Histology and Persistence of Various Injectable Filler Substances for Soft Tissue Augmentation. Aesthetic Plast Surg. 2003;27(5):354–66.
73. Pant R, Firmal P, Shah VK, Alam A, Chattopadhyay S. Epigenetic Regulation of Adipogenesis in Development of Metabolic Syndrome. Front Cell Dev Biol. 2021;8:619888.
74. Ruiz-Ojeda F, Rupérez A, Gomez-Llorente C, Gil A, Aguilera C. Cell Models and Their Application for Studying Adipogenic Differentiation in Relation to Obesity: A Review. Int J Mol Sci. 2016;17(7):1040.
75. Nobusue H, et al. Regulation of MKL1 via actin cytoskeleton dynamics drives adipocyte differentiation. Nat Commun. 2014;5(1):3368.
76. Warnke I, Goralczyk R, Fuhrer E, Schwager J. Dietary constituents reduce lipid accumulation in murine C3H10 T1/2 adipocytes: A novel fluorescent method to quantify fat droplets. Nutr Metab. 2011;8(1):30.
77. Yu G, et al. Yield and characterization of subcutaneous human adipose-derived stem cells by flow cytometric and adipogenic mRNA analyzes. Cytotherapy. 2010;12(4):538–46.

78. Khademhosseini A, Langer R. Microengineered hydrogels for tissue engineering. Biomaterials. 2007;28(34):5087–92.

79. Gogg S, Nerstedt A, Boren J, Smith U. Human adipose tissue microvascular endothelial cells secrete PPARγ ligands and regulate adipose tissue lipid uptake. JCI Insight. 2019;4(5):e125914.

# Figures

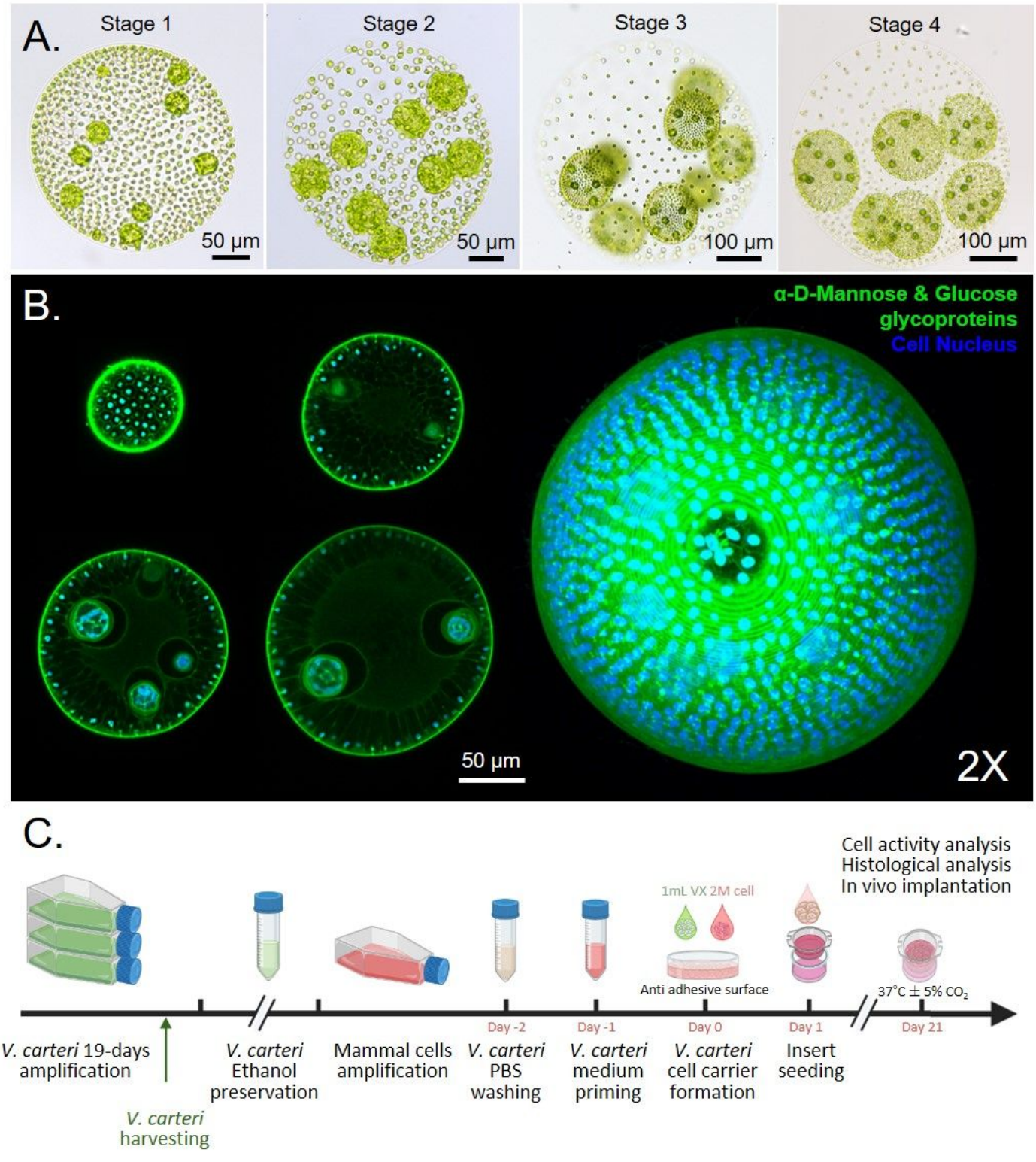

## Figure 1

**Processing of the algal spherical materialto engineer macrotissues.** A. Development of a *V. carteri* spheroid from juvenile to adult stage. *V. carteri* juvenile spheroid present ~2000 biflagellated somatic cells on their surface and up to 16 embryo cells termed as "gonidia" in their core. While the overall diameter of a juvenile spheroid continuously expands by extracellular matrix deposition, its unicellular algal embryo progressively divides symmetrically and then asymmetrically, leading to cell differentiation of somatic cells, which will constitute the external membrane, and gonidia progenitor cells that will grow as future daughter spheroids. Once both the adult and its daughters' spheroids reach a critical diameter, the juvenile hatch and are discharged; B. Observation of *V. carteri*'s overall structuration and compartmentation established by a highly organised intertwinned network of algal glycoproteins. Representative Z-stack and reconstructed 3D images of a stage 2 *V. carteri* spheroids labelled for glycoproteins with α-D-Mannose and Glucose sugar groups and DNA content with Concanavalin A (Green) and DAPI; C. Experimental procedure for the formation of *V. carteri* living building blocks-based macrotissues.

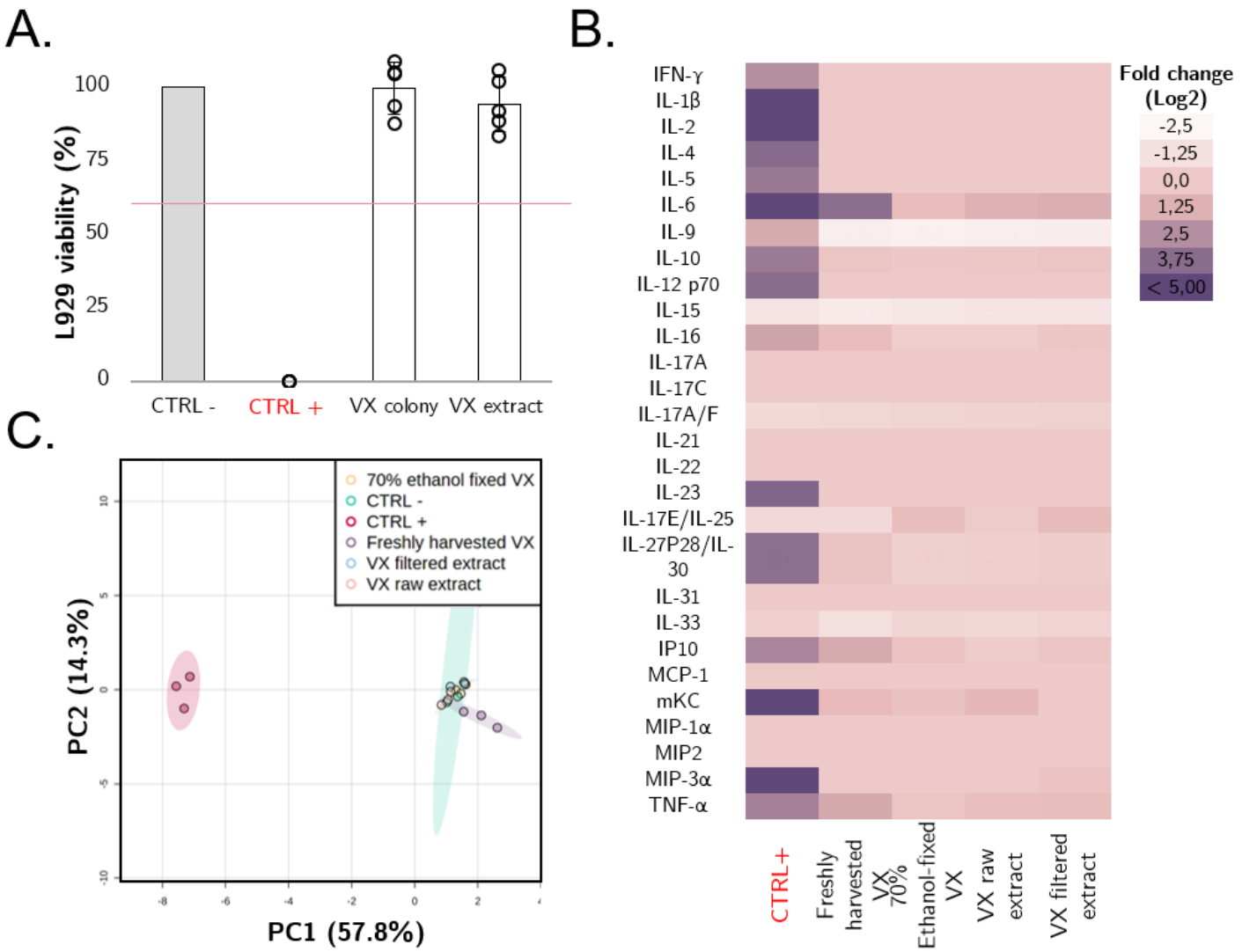

## Figure 2

***V. carteri*material *in vitro* biocompatibility analysis.** A. *V. carteri*cytotoxicity evaluation adapted from ISO 10993 standards (N=5), B. J774.2 murine macrophages inflammatory secretome upon *V. carteri* (VX) exposition. The supernatant cytokine and chemokine concentration upon J774.2 macrophage 24h-exposure were measured by Meso Scale Discovery, expressed as a Log2-fold change of the non-treated control and represented as a heatmap (N=3). When below or above the detection range, the concentrations were replaced by threshold values. A 2 µg/mL LPS solution was used as a positive control (CTRL+), C. PCA analysis of the *V. carteri*-induced macrophage secretome in regards to both untreated (CTRL-) and treated (CTRL+) controls. The supernatant cytokine and chemokine concentrations were processed for normalization and PCA analysis with Metaboanalysis software [22].

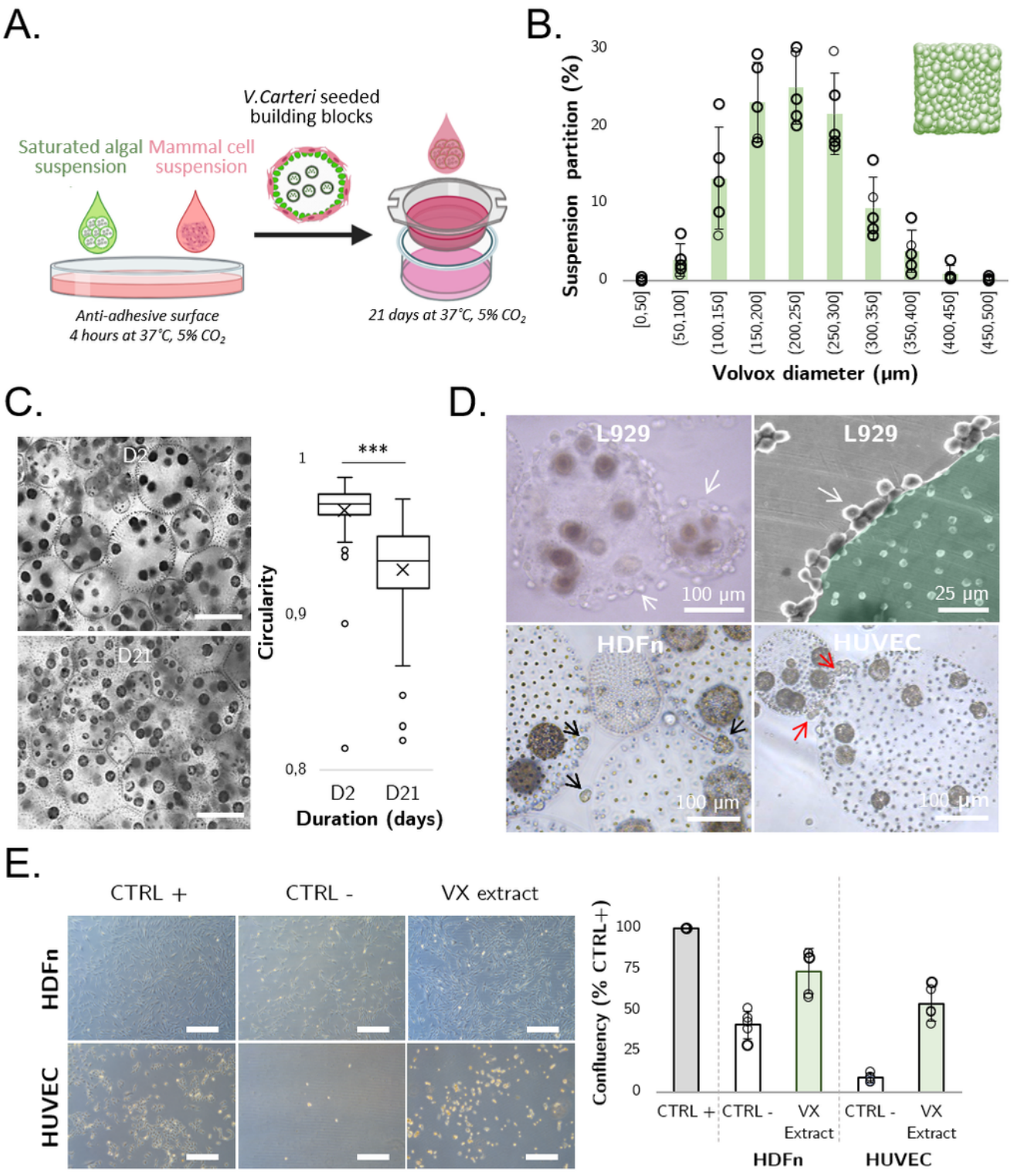


## Figure 3

**Production of compactable and deformable seeded *V. carteri* living building blocks.** A. Living building blocks formation principle, B. Normal distribution of *V. carteri* spheroids' diameter in the saturated algal suspension (N=5; Shapiro-Francia Test; W'= 0.9934). C. Evaluation of the algal suspension compaction and deformation of *V. carteri* spheroids by phase contrast microscopy through the determination of *V. carteri* colony circularity (N=3, n≥75, Welch t-test (***: p ≤0.001, scale bar: 250 µm). D. Observation of

various cell types *V. carteri* spheroids surface adhesion capacity. From left to right, contrast phase and environmental scanning electron microscopy (ESEM) observations of L929 adhered to the surface of *V. carteri* (white arrows), contrast phase observation of HDFn spheroid like structures (black arrows), and HUVEC cell chains (red arrows) adhered to the surface of *V. carteri* microalgae, E. Evaluation of *V. carteri* extract cell adhesion-promoting properties. Contrast-phase observation of HDFn and HUVEC cells upon 48h-seeding on culture treated, anti-adhesive or *V. carteri* extract coated surfaces (scale bar: 250 µm). PHANTAST pluging and Image J software were used to estimate cell confluency [20], [21](n≥3, Mann–Whitney U test (**: p ≤0.01)).

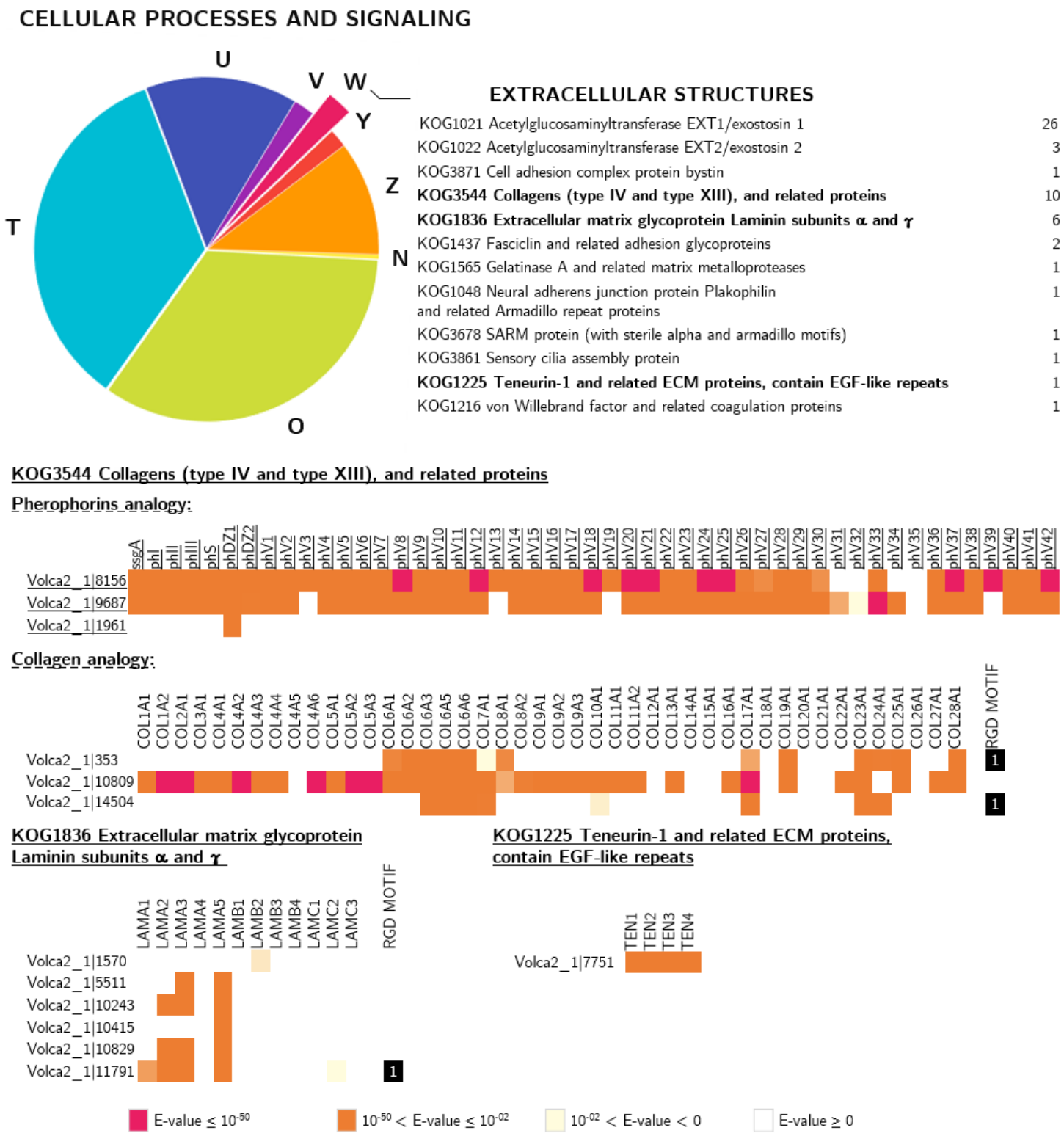


## Figure 4

**Investigation into the proteic foundation of *V. carteri*'s cell adhesion-promoting properties.** Using *V. carteri*'s previously published EuKaryotic Orthologous Groups (KOG) annotation analysis and predicted proteome [109], BlastP sequence homology analyses were performed against human extracellular matrix basic constituent sequences. Homology E-values between 0 and $10^{-50}$ were thus obtained and discarded in the form of a heat map (T: Signal transduction mechanisms, U: Intracellular trafficking, secretion, and

vesicular transport, V: Defense mechanisms, W: Extracellular structures, Y: Nuclear structure, Z: Cytoskeleton, ph: Pherophorin, COL: Collagen, LAM: Laminin, TEN: Teneurin, GH: Growth hormone, INS: Insulin, IGF: Insulin growth factor).

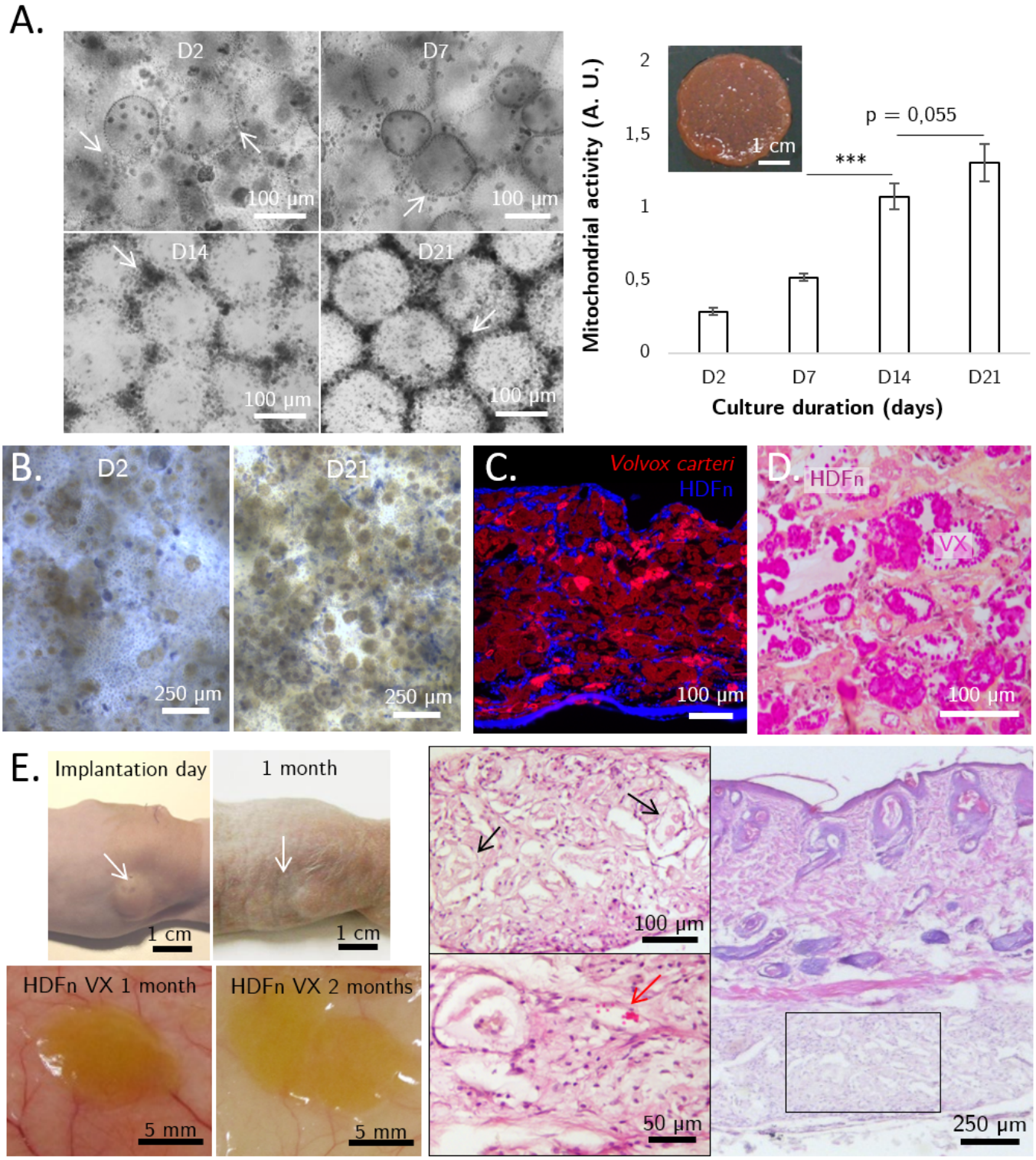


**Figure 5**

**Neonatal human dermal fibroblasts (HDFn) seeded *V. carteri* living building blocks *in vitro* self-assemble into modular macrotissue, early investigation of its *in vivo* physical stability and biocompatibility.** A. HDFn proliferation and densification (pointed by white arrows) monitoring at day 2, 7, 14 and 21 (N = 3, ANOVA analysis–Post Hoc Bonfferoni test (***: p < 0,001)) provided with a photograph of the macrotissue obtained after 21 days of culture**,** B. Monitoring of phosphatase alkaline activity in HDFn seeded in the *V. carteri*-based macrotissue system along the culture duration, C. DAPI-stained HDFn (blue) seeded Rhodamine-cross-linked *V. carteri* (red) living building blocks-based macrotissue epifluorescence observation, D. Histological analysis of HDFn-seeded Rhodamine-cross-linked *V. carteri* living building blocks-based macrotissue stained with Hematoxylin Eosine Safran, E. Post-implantation and 1-month follow-up photographs of the implant site (white arrow) are provided with macroscopic observation of *V. carteri* HDFn pseudotissue implant aspects at 1-month and 2-months post implantation, and a 1-month post-implantation histopathological examination of the implanted HDFn seeded *V. carteri* living building blocks-based macrotissue showing signs of algal degradation (black arrow) and tissue vascularization (red arrow).

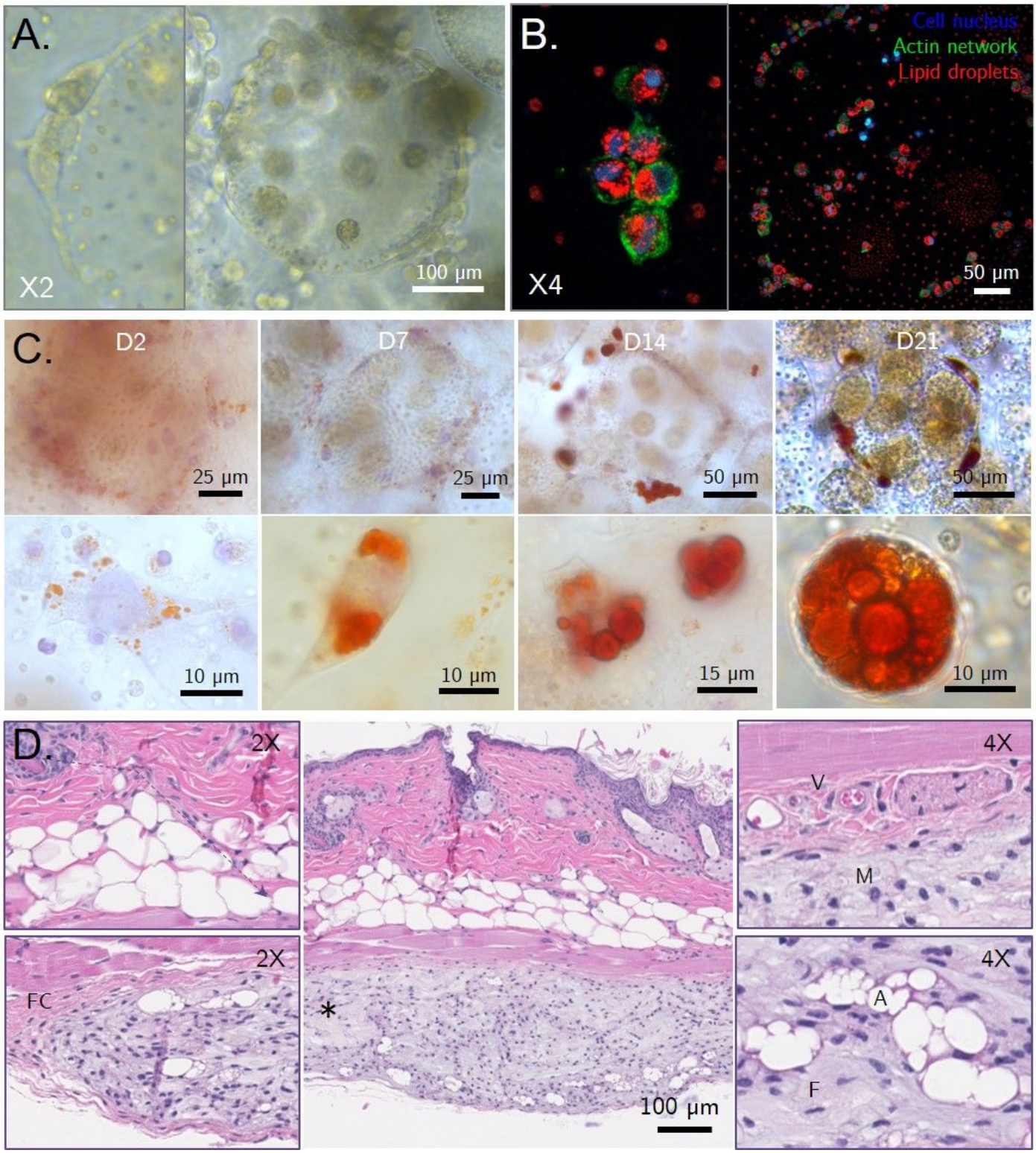


**Figure 6**

***V. carteri* demonstrates an adipogenic effect both *in vitro* and *in vivo*.** A. 48h human adipose-derived stem cells (hASC) seeded *V. carteri* building block constrast phase observation; B. Fluorescence confocal microscopy observation of 48h hASC seeded *V. carteri* building block showing the adhesion of hASC displaying adipogenic maturation signs in the production of numerous Oil red O stained lipid droplets; C. Monitoring of C3H/10T1/2 murine embryonic cells adipogenic differenciation upon culture in a *V. carteri*

living building blocks environment depicting both lipid droplets accumulation and expansion, D. Histopathological analysis of a 1-month post-implantation *V. carteri* only suspension subcutaneous injection in a nude athymic mouse model demonstrates histogenesis and adipogenic effects, exhibiting the development of a mesenchymal tissue including adipocytes islets (*: injected implant, FC: fibrous capsule, V: blood vessels, M: macrophages, A: adipocytes, F: fibroblasts, purple arrow : cellular infiltration).

## Supplementary Files

This is a list of supplementary files associated with this preprint. Click to download.

- AppendixA.docx